Efficient Robust Design with Stochastic Expansions

Yi Zhang and Serhat Hosder

Abstract This chapter describes the application of a computationally efficient uncertainty quantification approach, non-intrusive polynomial chaos (NIPC)-based stochastic expansions, for robust design under mixed (aleatory and epistemic) uncertainties and demonstrates this technique on robust design of a beam and on robust aerodynamic optimization. The approach utilizes stochastic response surfaces obtained with NIPC methods to approximate the objective function and the constraints in the optimization formulation. The objective function includes the stochastic measures, which are minimized simultaneously to ensure the robustness of the final design to both aleatory and epistemic uncertainties. The results of the optimization case studies show the computational efficiency and accuracy of the robust design with stochastic expansions, which may be applied to any stochastic optimization problem in science and engineering.

Keywords Aerodynamics · Optimization · Uncertainty quantification · Robust design · Stochastic expansions · Computational fluid dynamics

1 Introduction

Uncertainties are generally ubiquitous in the analysis and design of highly complex engineering systems, such as aerospace systems. Uncertainties can arise due to ignorance, lack of knowledge, and incomplete information in physical modeling (e.g., epistemic uncertainty in turbulence models) and from inherent variations in the systems (e.g., aleatory uncertainty in operating conditions). It is important to consider these uncertainties in engineering design. Robust design [1, 2] is a methodology for improving the quality of a product by minimizing the impact of uncertainties on the product performance. The objective is to optimize the mean performance while minimizing the variation of performance caused by various uncertainties. Many studies of robust design have been investigated in the past [3–12]. A comprehensive survey of robust optimization approaches is given by Beyer and Sendhoff [13].

Y. Zhang · S. Hosder (✉)
Department of Mechanical and Aerospace Engineering, Missouri University of Science and Technology, Rolla, MO, USA
e-mail: hosders@mst.edu

S. Koziel, L. Leifsson (eds.), *Surrogate-Based Modeling and Optimization*,
DOI 10.1007/978-1-4614-7551-4_11,

One very important component of robust design is the uncertainty quantification (UQ), which may increase the computational expense of the design process significantly compared to the computational work of deterministic optimization, especially when high-fidelity analysis tools are used to improve accuracy. Therefore, it is important to develop and implement computationally efficient robust design methodologies while keeping the desired accuracy level in the optimization process.

The goal of UQ is to determine how random variation (aleatory) and lack of knowledge (epistemic) affect the sensitivity, performance, or reliability of the system that is being modeled. Various studies have been made on the topic of propagating aleatory uncertainty through Monte Carlo sampling (MCS) [14–18], expansion-based methods (e.g., Taylor series [19–22] and perturbation methods [23–25]) and non-intrusive polynomial chaos (NIPC) expansions [26–28], and propagating epistemic uncertainty through interval analysis and evidence theory [29–34].

MCS is the most comprehensive (but expensive) UQ approach for evaluating statistical moments and the reliability and quality of the system response. It is a method for iteratively evaluating a deterministic model using sets of random numbers as inputs. This method is often used when the model is complex or nonlinear, or when it involves a large number of uncertain parameters. M.G. Cox et al. [16] worked on using MCS to determine the probability density function (PDF) of the output quantities. L.Y. Zhao et al. investigated UQ of a flapping airfoil with stochastic velocity deviations by using a classic Monte Carlo method to numerically investigate the responses of the time-averaged thrust coefficient and the propulsive efficiency with respect to a stochastic flight velocity deviation under Gaussian distributions [17, 18]. Y.P. Ju et al. conducted studies on multi-point robust design optimization of wind turbine airfoils under geometric uncertainty where the MCS technique was used for simulating the geometric uncertainty in the robust optimization [35]. Although MCS is the most popular sampling-based method, it requires thousands of computational simulations (e.g., computational fluid dynamics (CFD) and finite element analysis (FEA)) to obtain accurate results. It is extremely expensive and cannot be made affordable for complex engineering simulations, so it is often used as a benchmark for verification of UQ analysis when other methods are used.

Expansion-based UQ is used to estimate the statistical moments (e.g., mean, variance, etc.) of the system response with a small perturbation to simulate the effect of the input uncertainty. The Taylor series and perturbation method are two main expansion-based UQ approaches. The Taylor series is a series expansion of a function about a point that is used to approximate a function with a Taylor polynomial. For example, the first-order reliability method (FORM) uses the first-order Taylor expansion (linearization) to approximate the uncertainty in the output [19]. There have also been some studies on Taylor series expansion techniques and applications in physics [20–22]. The perturbation method is used to find an approximate solution to a problem which cannot be solved by traditional analytical methods. It allows the simplification of complex mathematical problems [23–25]. Both Taylor series and perturbation methods have advantages when dealing with relatively small input variability and outputs that do not express high nonlinearity. However, most real-life problems require much more difficult mathematical models, such as nonlinear

differential equations. Therefore, Taylor series and perturbation methods will not be a good option for uncertainty propagation in these cases.

The NIPC expansion is a spectral-based technique for UQ that has been used recently for numerous physical models, such as elasticity and fluid mechanics [36–38]. Some studies conducted by Eldred et al. [27, 28] introduced efficient stochastic expansions based on NIPC for UQ. In their study, they used Legendre and Hermite orthogonal polynomials to model the effect of uncertain variables described by uniform and normal probability distributions, respectively, and used Legendre orthogonal polynomials to model the effect of epistemic uncertainties. The accuracy and the computational efficiency of the NIPC method applied to stochastic problems with multiple uncertain input variables were investigated by Hosder et al. [39–41].

The non-probabilistic approaches which are used for epistemic UQ include interval analysis and evidence theory. Several studies have been conducted on epistemic uncertainty propagation [29–31]. The simplest way to propagate epistemic uncertainty is by interval analysis [32–34]. In interval analysis, it is assumed that nothing is known about the uncertain input variables except that they lie within certain intervals. L.P. Swiler and T.L. Paez [32, 33] examined three methods in propagating epistemic uncertainty: interval analysis, Dempster–Shafer evidence theory, and second-order probability, and demonstrated examples of their use on a problem in structural dynamics. They also examined the use of surrogate methods in epistemic analysis, both surrogate-based optimization in interval analysis and the use of polynomial chaos expansions to provide upper and lower bound approximations. From their studies, it was proved that interval analysis can be effective in the quantification of epistemic uncertainty.

Recently, there have been some studies investigating the topic of mixed (aleatory and epistemic) uncertainty propagation. Eldred et al. [42] proposed using second-order probability for estimating the effect of mixed uncertainties. This method was used to separate the aleatory and epistemic uncertainties into inner and outer sampling loops, respectively. Moreover, they applied this method to a cantilever beam design problem which was represented by two simple analytical functions. They utilized these analytical functions to represent ideal test cases, since they were inexpensive to evaluate. Therefore, this study provided an analytical reference for validating codes used for mixed aleatory and epistemic UQ. Bettis and Hosder applied the NIPC approach to the propagation of mixed uncertainties in hypersonic reentry problems [41, 43].

Most of the previous stochastic design studies focused on optimization under aleatory uncertainties which utilized different approaches for uncertainty propagation [3–12, 44]. Among these studies, Eldred [44] formulated and investigated design under aleatory uncertainty with stochastic expansions. Dodson and Parks utilized polynomial chaos expansions for robust airfoil design under aleatory input uncertainties [45]. B.D. Youn et al. also developed a robust design optimization with epistemic uncertainty. They proposed a new metric for product quality loss which was defined for epistemic uncertainty using the analogy between the probability and possibility theories. For the epistemic uncertainty, the maximum likely value and equivalent variation were employed to define the new metric for the product

quality loss in three different types of robust objectives [46]. A number of robust design studies have considered both aleatory and epistemic uncertainties, such as the work by Eldred [47], and Du et al. [48], who used a double-loop Monte Carlo sampling approach to determine the statistics of the response given in their model problems.

In this chapter, we describe a computationally efficient approach for robust aerodynamic optimization under aleatory (inherent) and epistemic (model-form) uncertainties using stochastic expansions based on the NIPC method [49]. In the context of aerodynamic shape optimization, robust design implies that the performance (such as the lift-to-drag ratio) of the final configuration should be insensitive to the uncertainties in the operating conditions (e.g., free-stream Mach number). Furthermore, the final design should be relatively insensitive to the physical modeling uncertainties in the computational tools used for aerodynamic analysis such as the computational fluid dynamics (CFD) codes.

The chapter is organized as follows. Section 2 describes the details of the robust design formulation with stochastic expansions. In Sect. 3, the methodology is applied to a model problem involving the design of a beam, and Sect. 4 describes an application to airfoil design at transonic flow conditions. The chapter is summarized in Sect. 5.

2 Robust Design with Stochastic Expansions

This section gives the details of different robustness measures for a system depending on the input uncertainty type, as well as the utilization of stochastic expansions in robust optimization.

2.1 Formulation of Robust Optimization

Following Du et al. [48], we describe the following robust measures: (1) purely aleatory (inherent) input uncertainty, (2) purely epistemic input uncertainty, and (3) mixed (aleatory and epistemic) input uncertainty.

2.1.1 Aleatory Uncertainties Only

If there are only aleatory uncertainties as input variables, the response R can be described as a function of $\mathbf{S}_a = (S_{a_1}, S_{a_2}, \ldots, S_{a_{N_a}})$, which is the vector consisting of N_a aleatory uncertainties; this vector can include both aleatory design variables ($\mathbf{X}_a$) and aleatory parameters ($\mathbf{P}_a$). In a design study, the aleatory uncertainty can be imposed on the design variables through the statistical distribution parameters that define them (e.g., mean and variance), which vary in the design space. Figure 1

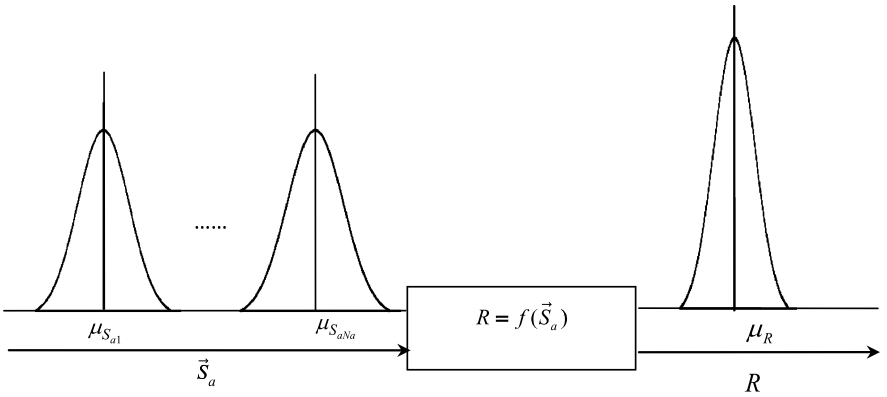

Fig. 1 Robustness estimation of response in the presence of aleatory uncertainties only

shows the propagation of input aleatory uncertainties through the simulation code and the uncertainty of the response, $R = f(\mathbf{S}_a)$. For a probabilistic output uncertainty, the mean and the variance of R can be calculated by

$$\mu_R = E(R) = \int_{\Omega} R(\mathbf{S}_a)\rho(\mathbf{S}_a)\, d\mathbf{S}_a, \tag{1}$$

$$\sigma_R^2 = E\left[(R - \mu_R)^2\right] = \int_{\Omega} \left(R(\mathbf{S}_a) - \mu_R\right)^2 \rho(\mathbf{S}_a)\, d\mathbf{S}_a, \tag{2}$$

where $\rho(\mathbf{S}_a)$ represents the joint PDF of $\mathbf{S}_a$, and Ω stands for the support region of $\mathbf{S}_a$. For this case, the variance (or the standard deviation, σ) of R is considered as the robustness measure.

2.1.2 Epistemic Uncertainties Only

If there are only epistemic uncertainties as input, the response will be a function of epistemic uncertainty vector $\mathbf{S}_e = (S_{e_1}, S_{e_2}, \ldots, S_{e_{N_e}})$, which may include epistemic design variables ($\mathbf{X}_e$) and epistemic parameters ($\mathbf{P}_e$) in general. In a design study, the epistemic uncertainty can be imposed on the design variables through the parameters that define them (e.g., average and the limits of the interval), which vary in the design space. The relationship between input epistemic uncertainties and response $R = f(\mathbf{S}_e)$ is shown in Fig. 2. The midpoint ($\overline{R}$) and width (δR) of interval R are the most relevant statistics of response R for this case, and are given by

$$\overline{R} = \frac{1}{2}(R_L + R_U), \tag{3}$$

$$\delta R = R_U - R_L, \tag{4}$$

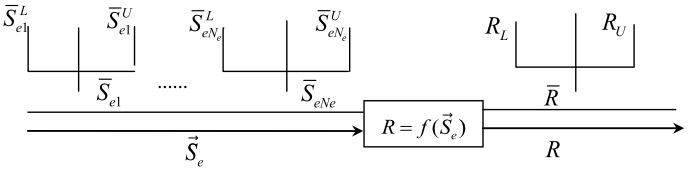

Fig. 2 Robustness estimation of response in the presence of epistemic uncertainties only

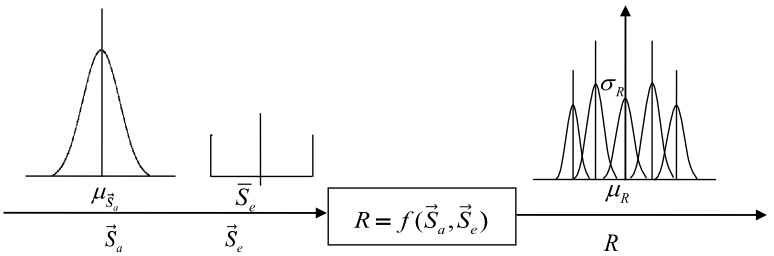

Fig. 3 Robustness estimation of response in the presence of mixed uncertainties

respectively, where R_U and R_L represent the upper bound and lower bound of R. For this case, the robustness of the response is assessed by δR. For robust optimization, δR should be as low as possible, while $\overline{R}$ is equal to the desired value.

2.1.3 Mixed Uncertainties (Both Aleatory and Epistemic Uncertainties)

When both aleatory uncertainties $\mathbf{S}_a = (S_{a_1}, \ldots, S_{a_{N_a}})$ and epistemic uncertainties $\mathbf{S}_e = (S_{e_1}, S_{e_2}, \ldots, S_{e_{N_e}})$ exist as input variables, the response R becomes a function of both types of uncertainty, $R = f(\mathbf{S}_a, \mathbf{S}_e)$, as shown in Fig. 3.

For this case, the uncertainty of R will be in the form of a family of probability distributions, each due to the aleatory input uncertainties at a fixed value of the epistemic input uncertainty vector. The intervals at each probability level will reflect the effect of epistemic uncertainties on R. The average mean value of R is calculated by

$$\overline{\mu}_R = \frac{1}{2}\left(\mu_R^{\max} + \mu_R^{\min}\right), \tag{5}$$

where $\mu_R^{\max}$ and $\mu_R^{\min}$ are the maximum and minimum means of response R, respectively. The average value of the standard deviation of R ($\overline{\sigma}_R$) is obtained by

$$\overline{\sigma}_R = \frac{1}{2}\left(\sigma_R^{\max} + \sigma_R^{\min}\right), \tag{6}$$

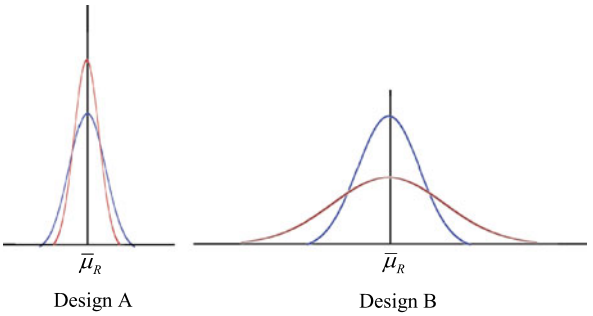

Fig. 4 Robustness assessment of mixed uncertainty design

where $\sigma_R^{\max}$ and $\sigma_R^{\min}$ are the maximum and minimum standard deviations of response R, respectively. The difference between $\sigma_R^{\max}$ and $\sigma_R^{\min}$ is computed by

$$\delta\sigma_R = \sigma_R^{\max} - \sigma_R^{\min}. \tag{7}$$

In a design study, the average standard deviation $\overline{\sigma}_R$ can be used as a robustness measure for aleatory input uncertainties ($\mathbf{S}_a$), whereas the standard deviation difference $\delta\sigma_R$ can be used as the robustness measure for epistemic uncertainties ($\mathbf{S}_e$). Note that one may also consider alternative measures for robustness to aleatory input uncertainties in the presence of mixed uncertainties. One approach will be to consider the maximum value of the standard deviation as a conservative measure, which in turn can be used in the robust optimization formulation described below.

2.1.4 Robust Optimization Formulation Under Mixed Uncertainties

To achieve a robust design in the presence of aleatory and epistemic uncertainties, both a lower value of $\overline{\sigma}_R$ and a lower value of $\delta\sigma_R$ are desired. To illustrate this, let us consider two designs (A and B) with performances (i.e., responses) having two different families of probability distributions represented by one blue and one red curve in Fig. 4. From these distributions, it is obvious that $\overline{\sigma}_R$ of design A is less than that of design B, which indicates that design A is more robust than design B when only randomness of the input is considered. Now comparing $\delta\sigma_R$ for the two designs, it can be seen that design A has a smaller difference between the distribution variances, indicating that it is also more robust to epistemic uncertainties. From the above discussion and following the formulation of Du et al. [48], a composite (weighted sum) objective function for robust optimization under mixed uncertainties can be written as

$$F(\mathbf{X}_d, \mathbf{S}_a, \mathbf{S}_e) = w_1\overline{\mu}_R + w_2\overline{\sigma}_R + w_3\delta\sigma_R, \tag{8}$$

where $\mathbf{X}_d$ is the deterministic design variable vector, $\mathbf{S}_a = \{\mathbf{X}_a, \mathbf{P}_a\}$, and $\mathbf{S}_e = \{\mathbf{X}_e, \mathbf{P}_e\}$. The values of the weight factors w_1, w_2, and w_3 should be chosen based on

the emphasis on the contribution of each term to the objective function by also considering the order of magnitude of each term. While minimizing F, a feasible design should also satisfy the inequality constraints $g_i(\mathbf{X}_d, \mathbf{S}_a, \mathbf{S}_e)$ $(i = 1, 2, \ldots, N_g)$ and the side constraints for aleatory design variables $\mathbf{X}_a$ (specified by the lower and the upper limits of the mean of the each aleatory variable), epistemic design variables $\mathbf{X}_e$ (specified by the lower and the upper limits of the epistemic variable), and the deterministic design variables $\mathbf{X}_d$. Under mixed uncertainties, a conservative form of the satisfaction of the inequality constraints can be written as $\mu_{gi}^{\max} + \beta\sigma_{gi}^{\max} \leq 0$, where $\mu_{g_i}^{\max}$ and $\sigma_{g_i}^{\max}$ are the maximum of the mean and the maximum of the standard deviation of the constraint function g_i, respectively. Here β_i is a positive constant which denotes the probability of constraint satisfaction.

In summary, the overall formulation for robust design optimization under aleatory and epistemic uncertainties can be written as:

$$
\begin{aligned}
&\text{Minimize} \quad && w_1\overline{\mu}_R + w_2\overline{\sigma}_R + w_3\delta\sigma_R \\
&\text{S.t.} \quad && \mu_{g_i}^{\max} + \beta_i\sigma_{g_i}^{\max} \leq 0, \quad i = 1, 2, \ldots, N_g \\
& && X_{d_j}^L \leq X_{d_j} \leq X_{d_j}^U, \quad j = 1, 2, \ldots, N_d \\
& && X_{e_k}^L \leq X_{e_k} \leq X_{e_k}^U, \quad k = 1, 2, \ldots, N_e \\
& && \mu_{X_{a_m}}^L \leq \mu_{X_{a_m}} \leq \mu_{X_{a_m}}^U, \quad m = 1, 2, \ldots, N_a.
\end{aligned}
\tag{9}
$$

2.2 Stochastic Expansions for Response Surface Modeling

For the robust optimization methodology described in this chapter, we adopt stochastic expansions obtained with non-intrusive polynomial chaos (NIPC) due to its computational efficiency and accuracy in aleatory and epistemic uncertainty propagation, as shown in the previous studies [43, 50]. The stochastic expansions are used as response surfaces (i.e., surrogates of the response) in the optimization procedure and are used to approximate the stochastic objective function or the constraint functions. In the robust optimization problems, we use two different NIPC approaches, point-collocation NIPC and quadrature-based NIPC. Below we give the description of these NIPC methods.

2.2.1 Non-intrusive Polynomial Chaos

Non-intrusive polynomial chaos is derived from polynomial chaos theory, which is based on the spectral representation of the uncertainty. An important aspect of spectral representation of uncertainty is that one may decompose a random function (or variable) into separable deterministic and stochastic components. For example, for any response variable (i.e., R) in a stochastic optimization problem, one can

write

$$R(\boldsymbol{\xi}) \approx \sum_{j=0}^{P} \alpha_j \Psi_j(\boldsymbol{\xi}), \tag{10}$$

where α_j is the coefficient of each term in the expansion, and $\Psi_j(\boldsymbol{\xi})$ is the random basis function corresponding to the jth mode and is a function of the n-dimensional random variable vector $\boldsymbol{\xi} = (\xi_1, \ldots, \xi_n)$, which has a specific probability distribution. In theory, the polynomial chaos expansion given by Eq. (10) should include an infinite number of terms; however, in practice a discrete sum is taken over a number of output modes. For a total order expansion, the number of output modes is given by

$$N_t = P + 1 = \frac{(n+p)!}{n!p!}, \tag{11}$$

which is a function of the order of polynomial chaos (p) and the number of random dimensions (n). The basis function ideally takes the form of a multidimensional Hermite polynomial to span the n-dimensional random space when the input uncertainty is Gaussian (unbounded), which was first used by Wiener [51] in his original work of polynomial chaos. To extend the application of the polynomial chaos theory to the propagation of continuous non-normal input uncertainty distributions, Xiu and Karniadakis [52] used a set of polynomials known as the Askey scheme to obtain the "Wiener–Askey generalized polynomial chaos." The Legendre and Laguerre polynomials, which are among the polynomials included in the Askey scheme, are optimal basis functions for bounded (uniform) and semibounded (exponential) input uncertainty distributions, respectively, in terms of the convergence of the statistics. The multivariate basis functions can be obtained from the product of univariate orthogonal polynomials (see Eldred et al. [27]). If the probability distribution of each random variable is different, then the optimal multivariate basis functions can again be obtained by the product of univariate orthogonal polynomials employing the optimal univariate polynomial at each random dimension. This approach requires the input uncertainties to be independent standard random variables, which also allows the calculation of the multivariate weight functions by the product of univariate weight functions associated with the probability distribution at each random dimension. Detailed information on polynomial chaos expansions can be found in Walters and Huyse [53], Najm [54], and Hosder and Walters [55].

The objective of the stochastic methods based on polynomial chaos is to determine the coefficient of each term ($\alpha_j(\mathbf{x}, t)$ $(j = 0, 1, \ldots, P)$) in the polynomial expansion given by Eq. (10). The statistics of the response can then be calculated using the coefficients and the orthogonality of basis functions. The mean of the random solution is given by

$$\mu_R = E\big[R(\boldsymbol{\xi})\big] = \int_{\Omega} R(\boldsymbol{\xi}) \rho(\boldsymbol{\xi})\, d\boldsymbol{\xi} = \alpha_0, \tag{12}$$

which indicates that the zeroth mode of the expansion corresponds to the expected value or the mean of $R(\boldsymbol{\xi})$. Similarly, the variance of the distribution can be obtained

as

$$\sigma_R^2 = \mathrm{Var}\big[R(\boldsymbol{\xi})\big] = \int_{\Omega} \big(R(\boldsymbol{\xi}) - \mu_R\big)^2 \rho(\boldsymbol{\xi})\, d\boldsymbol{\xi} \tag{13}$$

or

$$\sigma_R^2 = \sum_{j=1}^{P} \big[\alpha_j^2 \langle \Psi_j^2 \rangle\big]. \tag{14}$$

In the above equations, we have used the fact that $\langle \Psi_j \rangle = 0$ for $j > 0$ and $\langle \Psi_i \Psi_j \rangle = \langle \Psi_j^2 \rangle \delta_{ij}$, where the inner product expression $\langle \cdots \rangle$ represents

$$\big\langle f(\boldsymbol{\xi}) g(\boldsymbol{\xi}) \big\rangle_{\boldsymbol{\xi}} = \int_{\Omega} f(\boldsymbol{\xi}) g(\boldsymbol{\xi}) \rho(\boldsymbol{\xi})\, d\boldsymbol{\xi} \tag{15}$$

written in terms of two generic functions $f(\boldsymbol{\xi})$ and $g(\boldsymbol{\xi})$ in the support region Ω of $\boldsymbol{\xi}$ with $\rho(\boldsymbol{\xi})$ as the weight function.

To model the uncertainty propagation in computational simulations via polynomial chaos with the intrusive approach, all dependent variables and random parameters in the governing equations are replaced with their polynomial chaos expansions. Taking the inner product of the equations (or projecting each equation onto the jth basis) yields $P+1$ times the number of deterministic equations which can be solved by the same numerical methods applied to the original deterministic system. Although straightforward in theory, an intrusive formulation for complex problems can be relatively difficult, expensive, and time-consuming to implement. To overcome these inconveniences associated with the intrusive approach, non-intrusive polynomial chaos formulations have been considered for uncertainty propagation.

Point-Collocation NIPC The point-collocation NIPC method starts with replacing the uncertain variables of interest with their polynomial expansions given by Eq. (10). Then, $N_t = P + 1$ vectors ($\boldsymbol{\xi}_j = \{\xi_1, \xi_2, \ldots, \xi_n\}_j$, $j = 0, 1, \ldots, P$) are chosen in random space for a given PC expansion with $P + 1$ modes, and the deterministic code is evaluated at these points. With the left-hand side of Eq. (10) known from the solutions of deterministic evaluations at the chosen random points, a linear system of equations can be obtained:

$$\begin{pmatrix} R(\overrightarrow{\xi_0}) \\ R(\overrightarrow{\xi_1}) \\ \vdots \\ R(\overrightarrow{\xi_P}) \end{pmatrix} = \begin{pmatrix} \Psi_0(\overrightarrow{\xi_0}) & \Psi_1(\overrightarrow{\xi_0}) & \cdots & \Psi_P(\overrightarrow{\xi_0}) \\ \Psi_0(\overrightarrow{\xi_1}) & \Psi_1(\overrightarrow{\xi_1}) & \cdots & \Psi_P(\overrightarrow{\xi_1}) \\ \vdots & \vdots & \ddots & \vdots \\ \Psi_0(\overrightarrow{\xi_P}) & \Psi_1(\overrightarrow{\xi_P}) & \cdots & \Psi_P(\overrightarrow{\xi_P}) \end{pmatrix} \begin{pmatrix} \alpha_0 \\ \alpha_1 \\ \vdots \\ \alpha_0 \end{pmatrix}. \tag{16}$$

The coefficients (α_j) of the stochastic expansion are obtained by solving the linear system of equations given above. The solution of the linear problem given by Eq. (16) requires N_t deterministic function evaluations. If more than N_t samples are chosen, then the overdetermined system of equations can be solved using the

least squares approach. Hosder et al. [56] investigated this option on model stochastic problems by increasing the number of collocation points in a systematic way through the introduction of an oversampling ratio (*OSR*) defined as the number of samples divided by N_t. Based on a study of different model problems, they suggested an effective *OSR* of 2.0. Point-collocation NIPC has the advantage of flexibility on the selection of collocation points. With the proper selection of collocation points, it has been shown that point-collocation NIPC can produce highly accurate stochastic response surfaces with computational efficiency [56]. In the model problems considered in this study, we use Latin hypercube sampling with an oversampling ratio of 1 or 2 to choose the collocation points. The number of response evaluations will be $OSR \times N_t$ when point-collocation NIPC is used to construct the stochastic response surface.

Quadrature-Based NIPC With the quadrature-based NIPC method, stochastic expansion coefficients α_j (see Hosder and Walters [55] for details) can be obtained by using the equation

$$\alpha_j = \frac{\langle R, \Psi_j(\boldsymbol{\xi}) \rangle}{\langle \Psi_j^2(\boldsymbol{\xi}) \rangle} = \frac{1}{\langle \Psi_j^2(\boldsymbol{\xi}) \rangle} \int_{\Omega} R \Psi_j(\boldsymbol{\xi}) \rho(\overrightarrow{\xi}) \, d\overrightarrow{\xi} . \tag{17}$$

Since the denominator $\langle \Psi_j^2 \rangle$ in Eq. (17) can be computed analytically for multivariate orthogonal polynomials, the main purpose is to compute the coefficients by estimating the numerator $\langle R, \Psi_j \rangle$ in Eq. (17). In the quadrature-based NIPC method, the approximation of multidimensional integrals can be achieved by applying a tensor product of one-dimensional quadrature rules. The Gaussian quadrature points are precisely the roots of the orthogonal polynomial on the same interval (the support region of the uncertain variable $\boldsymbol{\xi}$), and a weighting function is associated with the given uncertainty distribution (i.e., Gauss–Legendre and Gauss–Hermite quadrature for expansions on uniform and normal random variables, respectively). For one-dimensional integrals, if the polynomial chaos expansion degree is p, then the minimum Gaussian points required for the exact estimation of the integral will be $p + 1$ (with the assumption that the response R can be represented exactly with a polynomial expansion of p), since the p-point Gaussian quadrature rule will yield an exact result for polynomials of degree $2p - 1$ or less, and the polynomial degree of the product of function estimation and the basis polynomials in the numerator in Eq. (17) will be $2p$. Therefore, the number of response evaluations will be $(p + 1)^n$ when quadrature-based NIPC is used to construct the response surface as a function of n expansion variables. For multidimensional problems with a large number of uncertain variables, the computational cost of this method will be significant due to its exponential growth with the number of random dimensions. For these cases, an alternative approach for more efficient evaluation of the multidimensional integrals will be to use sparse tensor product spaces instead of full tensor products of Gauss quadrature points to cover the multidimensional random space (see Eldred et al. [27, 44] for details).

2.3 Utilization of Stochastic Expansions for Robust Design

The methodology described in this chapter employs the stochastic response surfaces obtained with NIPC methods described above. While constructing the stochastic response surfaces, a combined expansion approach is utilized, which expands the polynomials as a function of uncertain design variables and parameters (aleatory and epistemic), as well as the deterministic design variables. We will describe this approach and robust optimization with stochastic expansions in the following sections.

2.3.1 Formulation with Combined Expansions

With the introduction of deterministic design variables ($\mathbf{X}_d$), design variables with epistemic uncertainty ($\mathbf{X}_e$), parameters with epistemic uncertainty ($\mathbf{P}_e$), design variables with aleatory uncertainty ($\mathbf{X}_a$), and parameters with aleatory uncertainty ($\mathbf{P}_a$), a combined stochastic expansion of R is written as

$$R\big(\mathbf{X}_a(\boldsymbol{\xi}_{xa}), \mathbf{P}_a(\boldsymbol{\xi}_{pa}), \mathbf{X}_e(\boldsymbol{\xi}_{xe}), \mathbf{P}_e(\boldsymbol{\xi}_{pe}), \mathbf{X}_d(\boldsymbol{\xi}_d)\big) = \sum_{j=0}^{P} \alpha_j \Psi_j(\boldsymbol{\xi}_{xa}, \boldsymbol{\xi}_{pa}, \boldsymbol{\xi}_{xe}, \boldsymbol{\xi}_{pe}, \boldsymbol{\xi}_d). \tag{18}$$

In this approach, multidimensional basis functions Ψ_j are derived from the tensor product of one-dimensional optimum basis functions for the aleatory uncertain parameters and design variables ($\mathbf{P}_a$ and $\mathbf{X}_a$) selected based on their input probability distributions (e.g., Hermite polynomials for normal uncertain variables, the Legendre polynomials for the epistemic uncertain parameters and design variables ($\mathbf{P}_e$ and $\mathbf{X}_e$), and the Legendre polynomials for the deterministic design variables ($\mathbf{X}_d$)). The selection of the Legendre polynomials as basis functions for the epistemic uncertainties and the design variables is due to their bounded nature ($\mathbf{P}_e^L \le \mathbf{P}_e \le \mathbf{P}_e^U$, $\mathbf{X}_e^L \le \mathbf{X}_e \le \mathbf{X}_e^U$, and $\mathbf{X}_d^L \le \mathbf{X}_d \le \mathbf{X}_d^U$) and should not be interpreted as a probability assignment to these variables. In Eq. (18), $\boldsymbol{\xi}_{xa}$ and $\boldsymbol{\xi}_{pa}$ correspond to standard aleatory random variable vectors associated with $\mathbf{X}_a$ and $\mathbf{P}_a$, whereas $\boldsymbol{\xi}_{xe}$, $\boldsymbol{\xi}_{pe}$, and $\boldsymbol{\xi}_d$ are the standard variables in the interval $[-1, 1]$, which are mapped from the associated intervals of $\mathbf{X}_e$, $\mathbf{P}_e$, and $\mathbf{X}_d$ via

$$\boldsymbol{\xi}_{xe} = \left(\mathbf{X}_e - \left(\frac{\mathbf{X}_e^L + \mathbf{X}_e^U}{2}\right)\right) \Big/ \left(\frac{\mathbf{X}_e^U - \mathbf{X}_e^L}{2}\right), \tag{19}$$

$$\boldsymbol{\xi}_{pe} = \left(\mathbf{P}_e - \left(\frac{\mathbf{P}_e^L + \mathbf{P}_e^U}{2}\right)\right) \Big/ \left(\frac{\mathbf{P}_e^U - \mathbf{P}_e^L}{2}\right), \tag{20}$$

$$\boldsymbol{\xi}_d = \left(\mathbf{X}_d - \left(\frac{\mathbf{X}_d^L + \mathbf{X}_d^U}{2}\right)\right) \Big/ \left(\frac{\mathbf{X}_d^U - \mathbf{X}_d^L}{2}\right). \tag{21}$$

Using the combined expansion given in Eq. (18), the mean and the variance of the response are obtained by evaluating the expectations over the aleatory uncertain variables ($\boldsymbol{\xi}_{xa}$ and $\boldsymbol{\xi}_{pa}$), which will be functions of standard epistemic design variables ($\boldsymbol{\xi}_{xe}$), standard epistemic parameters ($\boldsymbol{\xi}_{pe}$), and standard deterministic design variables ($\boldsymbol{\xi}_{d}$):

$$\mu_R(\boldsymbol{\xi}_{xe}, \boldsymbol{\xi}_{pe}, \boldsymbol{\xi}_{d}) = \sum_{j=0}^{P} \alpha_j \left\langle \Psi_j(\boldsymbol{\xi}_{xa}, \boldsymbol{\xi}_{pa}, \boldsymbol{\xi}_{xe}, \boldsymbol{\xi}_{pe}, \boldsymbol{\xi}_{d}) \right\rangle_{\boldsymbol{\xi}_{xa}, \boldsymbol{\xi}_{pa}}, \tag{22}$$

$$\sigma_R^2(\boldsymbol{\xi}_{xe}, \boldsymbol{\xi}_{pe}, \boldsymbol{\xi}_{d}) = \left(\sum_{j=0}^{P} \sum_{k=0}^{P} a_j a_k \langle \Psi_j \Psi_k \rangle_{\boldsymbol{\xi}_{xa}, \boldsymbol{\xi}_{pa}} \right) - \mu_R^2. \tag{23}$$

2.3.2 Robust Design Based on Stochastic Expansions

The flowchart of robust optimization under mixed uncertainties based on combined stochastic expansions is shown in Fig. 5. From Eqs. (22) and (23) it can be clearly seen that the mean and standard deviation of the response R (i.e., objective function F or constraint g_i) at a given design point are characterized by two bounds due to epistemic uncertainties with specified interval bounds $[\mathbf{X}_e^L, \mathbf{X}_e^U]$ and $[\mathbf{P}_e^L, \mathbf{P}_e^U]$. In other words, the mean and standard deviation of the output (response) will also be bounded by its maximum and minimum values. In our approach, we calculate $\mu_R^{\max}$, $\mu_R^{\min}$, $\sigma_R^{\max}$, and $\sigma_R^{\min}$ at a given design point through optimization using the analytical expressions of response statistics obtained with Eq. (22) and Eq. (23). Then, these values are used in the robust optimization formulation given by Eq. (9), which is performed with the sequential quadratic programing (SQP) method [57]. The whole procedure is repeated until the convergence is achieved. Note that when at least one design variable is uncertain (aleatory or epistemic), the stochastic response surfaces for the objective function and the constraints (if necessary) have to be reconstructed at each optimization iteration, since the uncertain design variables and the associated statistics are updated at each iteration, changing the bounds on which the response surfaces are created. On the other hand, if all design variables are deterministic and the uncertainties are associated with the problem parameters, only a single stochastic response surface for the objective function and a single response surface for each constraint function have to be constructed, since the bounds on the statistics of uncertain parameters and the bounds on the design variables are fixed and do not vary during the entire optimization process.

3 Model Problem: Robust Design of a Beam

In this model problem, which includes uncertainties in both design variables and parameters, we consider the robust design of a cantilever beam shown in Fig. 6 with

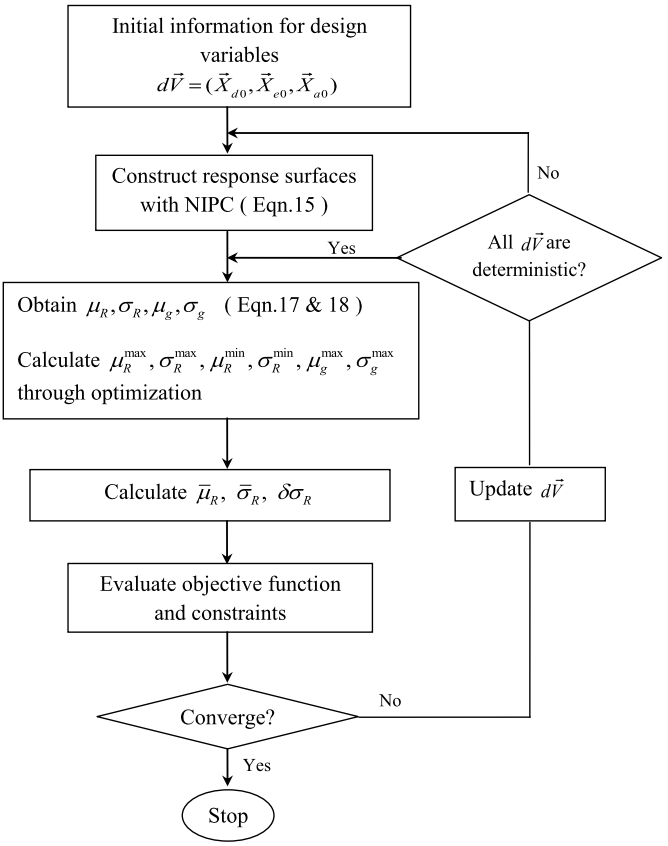

Fig. 5 Flowchart of the robust optimization process under mixed uncertainties with combined stochastic expansions

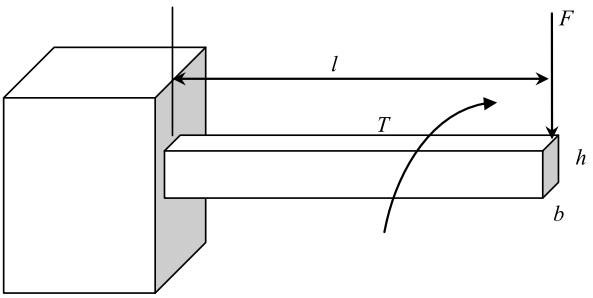

Fig. 6 Schematic of the beam design problem

length l, width b, and height h. The beam is subjected to a torque T and an external force F acting normal to the horizontal axis of the beam at its free end. The objective

Table 1 Design variables (DV) and parameters (P) with epistemic uncertainty (beam design model problem)

DV / P	lower limit	upper limit
$\overline{l}$ (DV)	$\overline{l} - 0.1\overline{l}$	$\overline{l} + 0.1\overline{l}$
F (P)	270 lb	330 lb

Table 2 Design variables (DV) and parameters (P) with aleatory uncertainty (beam design model problem)

DV / P	Mean	Standard deviation	Distribution
h (DV)	μ_h	$1\,\%\mu_h$	Normal
b (DV)	μ_b	$1\,\%\mu_b$	Normal
S (P)	100 kpsi	10 kpsi	Normal
T (P)	450 lb-in	50 lb-in	Normal

is to reduce the volume ($V = lbh$) of the beam while satisfying a stress constraint given by

$$g = \sqrt{\left(\frac{6FL}{bh^2}\right)^2 + 3\left[\frac{T}{b^2h}\left(3 + \frac{1.8b}{h}\right)\right]^2} - S \leqslant 0. \tag{24}$$

This equation represents the difference between the maximum equivalent stress of the beam and the yield strength S, which must be less than or equal to zero for a safe design. In this design problem, the external force F is considered as a parameter with epistemic uncertainty and the length of the beam l is treated as an epistemic design variable (Table 1). The external torque T and yield strength S are treated as parameters with aleatory uncertainty, whereas the width b and the height h of the beam are modeled as aleatory design variables with statistics given in Table 2. To ensure robustness of the design under epistemic and aleatory uncertainties, the objective function, which is the weighted sum of the average mean of the volume ($\overline{\mu}_V$), the average standard deviation of the volume ($\overline{\sigma}_V$), and the difference between the maximum and minimum standard deviation of the volume ($\delta\sigma_V$) should be minimized. The inequality constraint given by Eq. (24) should be satisfied at the worst case with a specified β value of 3. With the addition of the limits for the design variables, the robust design formulation for this problem is given as:

$$\begin{aligned} \min_d \quad & w_1\overline{\mu}_V + w_2\overline{\sigma}_V + w_3\delta\sigma_V \\ \text{s.t.} \quad & \mu_g^{\max} + \beta\sigma_g^{\max} \leq 0 \\ & 0.1 \leq \mu_h \leq 0.8 \\ & 0.1 \leq \mu_b \leq 0.4 \\ & 2 \leq \overline{l} \leq 20. \end{aligned} \tag{25}$$

Considering the magnitude of $\overline{\mu}_V$, $\overline{\sigma}_V$, and $\delta\sigma_V$, the weights in the multi-objective function are chosen as $w_1 = 1$, $w_2 = 100$, and $w_3 = 500$ to ensure equal contribu-

tions to the objective function from each term (i.e., scaling them to approximately the same order of magnitude).

For this problem, besides the stochastic response surface-based approach, robust optimization was also performed with double-loop Monte Carlo sampling (MCS), which was the approach used by Du et al. [48] to propagate the mixed uncertainties and obtain the maximum and minimum value of the response statistics used in the robust optimization formulation. After performing a convergence study based on the inner and outer loop samples, the desired accuracy with the double-loop MCS approach for the robustness measures was obtained with 500 epistemic variable samples in the outer loop and 10^5 aleatory variable samples in the inner loop. The convergence of the performance and robustness measures used in the objective function ($\bar{\mu}_V$, $\bar{\sigma}_V$, and $\delta\sigma_V$) obtained with quadrature-based and point-collocation NIPC with $OSR = 1$ and $OSR = 2$ was studied for different polynomial expansion orders at the optimum design point obtained with the Monte Carlo approach (Fig. 7). For the same robustness measures, the error values relative to the Monte Carlo results at each polynomial order are shown in Fig. 8. It is evident that the convergence is rapid for $\overline{\mu}_V$ and is achieved by the first-order expansion for all NIPC methods. The convergences for $\overline{\sigma}_V$ and $\delta\sigma_V$ are obtained at the second-order expansion. From Fig. 8, it can be seen that quadrature-based NIPC is more accurate than the point-collocation-based approach in terms of the error levels (especially for $\delta\sigma_V$) observed at the second-order expansion.

Based on the convergence results, the robust optimization was performed with stochastic response surfaces representing the objective function and the inequality constraint obtained with the NIPC approach utilizing a second-order polynomial expansion over aleatory and epistemic design variables and parameters. The two NIPC methods, point-collocation and quadrature-based, were implemented to obtain the stochastic response surfaces for comparison. The point-collocation method was performed with an OSR of 1 and 2. The number of original function evaluations required to construct a single response surface was 28 for the point-collocation method with $OSR = 1$ and 56 with $OSR = 2$. The quadrature-based method required 729 function evaluations. For this case, two response surfaces were constructed at each optimization iteration, one for the objective function and the other for the inequality constraint. The optimum design variable values obtained with the stochastic response surface based optimization again compare well with the result of the approach utilizing the double-loop MCS (Table 3) at a significantly reduced cost in terms of the total number of function evaluations, which include both the objective and constraint functions. Point-collocation NIPC is more efficient than quadrature-based NIPC for this problem, since the number of expansion variables ($n = 6$) is greater than the number of variables in the previous model problem ($n = 3$) and the computational cost of quadrature-based NIPC increases exponentially with the number of expansion variables for a given polynomial degree. An alternative approach to reduce the computational expense of the quadrature-based approach will be to implement sparse grid and cubature techniques, which may improve the computational efficiency significantly while retaining the accuracy of the original tensor product quadrature method. Table 4 presents the average mean, average standard

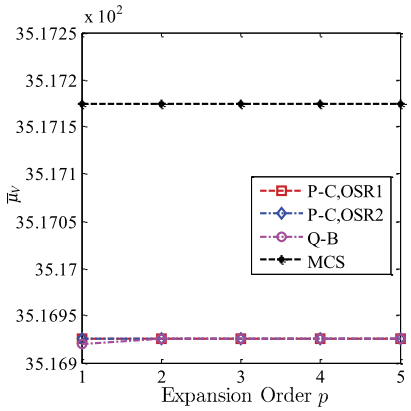

(a) Average mean of beam volume, $\bar{\mu}_V$

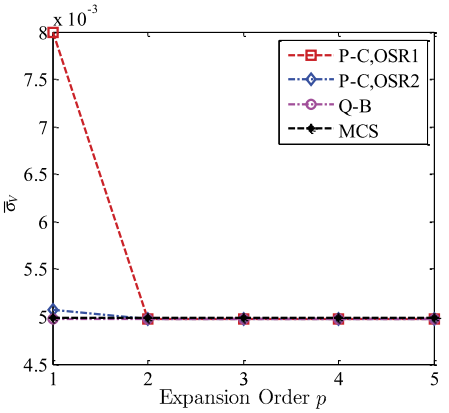

(b) Average standard deviation of beam volume, $\bar{\sigma}_V$

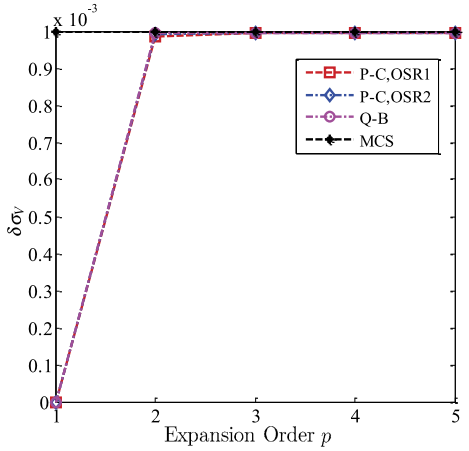

(c) Difference of standard deviation of beam volume, $\delta\sigma_V$

Fig. 7 Convergence of NIPC results as a function of expansion order for beam design model problem

deviation, and the standard deviation difference of the beam volume at the optimum design point; these are approximately the same for all the methods. The convergence histories of these terms are given in Fig. 9 for the optimization process with stochastic expansions. As can be seen from this figure, all three quantities are minimized simultaneously and converge to the same final values, which validates the described stochastic response surface based robust optimization approach. Another important observation made from this figure is that the quadrature-based approach seems to converge to the optimum robust design in terms of all measures at a lower number of iterations and in a more stable manner compared to the point-collocation-based

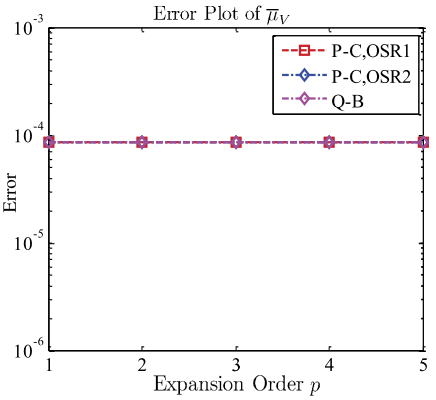

(a) Error of average mean of beam volume, $\bar{\mu}_V$

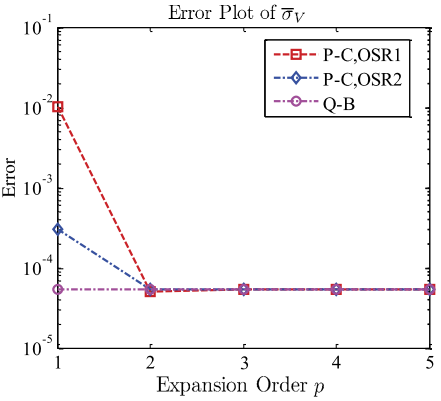

(b) Error of average standard deviation of beam volume, $\bar{\sigma}_V$

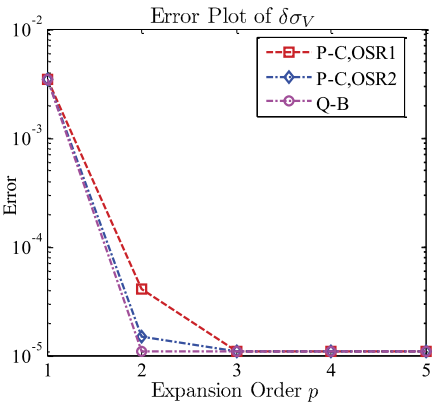

(c) Error of difference of standard deviation of beam volume, $\delta\sigma_V$

Fig. 8 Error convergence of NIPC results as a function of expansion order for beam design model problem

Table 3 Optimum design results of the beam problem (RS: response surface, Q-B: quadrature-based, P-C: point-collocation, MCS: Monte Carlo sampling, FE: function evaluations)

Method	$\{\mu_h, \mu_b, \bar{l}\}$ (in)	Total # of FE
MCS	{0.548, 0.327, 2.0}	23.5×10^8
Q-B	{0.542, 0.323, 2.0}	96,228
P-C, OSR = 1	{0.543, 0.324, 2.0}	3,696
P-C, OSR = 2	{0.542, 0.323, 2.0}	6,720

methods, especially the one with $OSR = 1$. This emphasizes another aspect of the importance of the accuracy of the stochastic response surfaces used in the robust

Table 4 Robustness assessment of the beam problem

Method	$\overline{\mu}_V$	$\overline{\sigma}_V$	$\delta\sigma_V$
MCS	3.55×10^{-1}	5.06×10^{-3}	1.01×10^{-3}
Q-B	3.50×10^{-1}	4.96×10^{-3}	9.91×10^{-4}
P-C, OSR = 1	3.52×10^{-1}	4.97×10^{-3}	9.86×10^{-4}
P-C, OSR = 2	3.50×10^{-1}	4.94×10^{-3}	9.88×10^{-4}

optimization approach in terms of the number of iterations to converge, which may influence the computational efficiency of the overall stochastic optimization process.

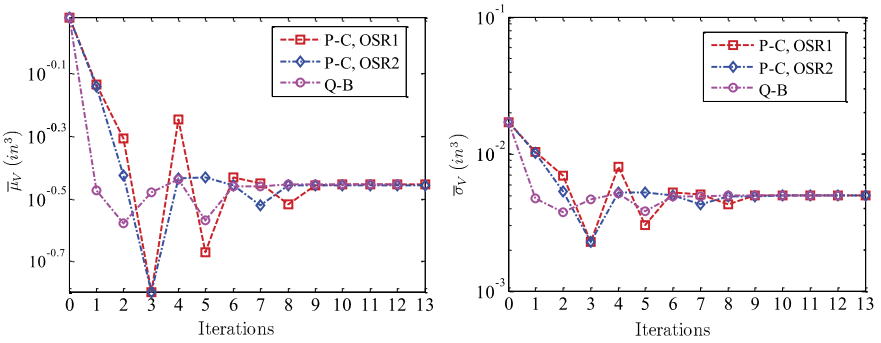

(a) Average mean of beam volume, $\bar{\mu}_V$

(b) Average standard deviation of beam volume, $\bar{\sigma}_V$

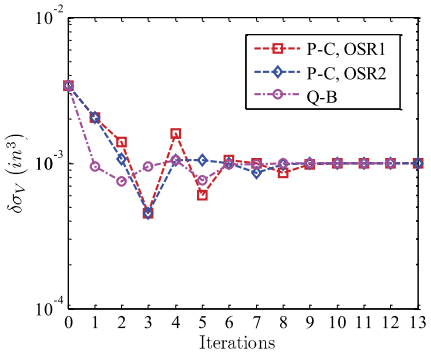

(c) Difference of standard deviation of beam volume, $\delta\sigma_V$

Fig. 9 The convergence history of average mean, average standard deviation, and the standard deviation difference of the beam volume for the optimization process with stochastic expansions

4 Application Example: Robust Airfoil Design

In this section, a computationally efficient approach for robust aerodynamic optimization under aleatory (inherent) and epistemic (model-form) uncertainties using stochastic expansions based on the point-collocation NIPC method is described. The deterministic CFD simulation model used in the optimization studies is described. Then the robust aerodynamic optimization formulations are given, followed by a discussion on the utilization of stochastic expansions in robust optimization. The results of two case studies are presented.

4.1 Computational Fluid Dynamics and Airfoil Shape Model

This section describes the elements of the CFD model, including the governing equations, numerical solution of the governing fluid flow equations (flow solver), the airfoil shape model, and meshing of the solution domain.

4.1.1 Governing Equations

The flow is assumed to be steady, two dimensional, compressible, and turbulent. The steady Reynolds-averaged Navier–Stokes (RANS) equations are taken as the governing fluid flow equations. The fluid medium is air, assumed to be an ideal gas, with the laminar dynamic viscosity (μ) described by Sutherland's formula (see, e.g., Ref. [58]). For modeling the turbulent kinematic eddy viscosity (ν_t), we use the turbulence model by Spalart and Allmaras [59]. The Spalart–Allmaras model, designed specifically for aerodynamic wall-bounded flows, is a one-equation model that solves a single conservation partial differential equation for the turbulent viscosity. This conservation equation contains convective and diffusive transport terms, as well as expressions for the production and dissipation of ν_t. The Spalart–Allmaras model is economical and accurate for attached wall-bounded flows and flows with mild separation and recirculation. However, the model may not be accurate for massively separated flows, free shear flows, and decaying turbulence. As described later, the turbulent viscosity is multiplied by a factor k to introduce the epistemic uncertainty in our robust optimization under mixed uncertainties problem. This is implemented in the solution through a user-defined function (UDF) which is dynamically loaded with the flow solver (described below) for each CFD simulation. The whole procedure is executed automatically through scripts.

4.1.2 Flow Solver

The flow solver is of implicit density-based formulation, and the fluxes are calculated by an upwind-biased second-order spatially accurate Roe flux scheme. Asymptotic convergence to a steady state solution is obtained for each case. Automatic solution steering is employed to gradually ramp up the Courant number and accelerate

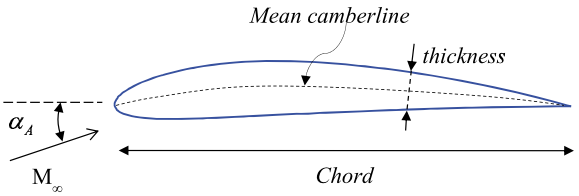

Fig. 10 A typical NACA four-digit airfoil section is shown. The free-stream flow is at Mach number M_∞, at an angle of attack α_A relative to the chord axis

convergence. Full multigrid initialization is used to get a good starting point. Numerical fluid flow simulations are performed using the computer code FLUENT [60].

The iterative convergence of each solution is examined by monitoring the overall residual, which is the sum (over all the cells in the computational domain) of the L^2 norm of all the governing equations solved in each cell. In addition to this, the lift and drag forces are monitored for convergence. The solution convergence criterion for the CFD runs is the one that occurs first of the following: a maximum residual of 10^{-6}, or a maximum number of iterations of 1,000.

4.1.3 Airfoil Geometry

In this work, we use the National Advisory Committee for Aeronautics (NACA) airfoil shapes. In particular, we use the NACA four-digit airfoil parameterization method, where the airfoil shape is defined by three parameters: c (the maximum ordinate of the mean camber line as a fraction of the chord), l_c (the chordwise position of the maximum ordinate as a fraction of the chord), and t (the thickness-to-chord ratio). The airfoils are denoted by NACA $mpxx$, where xx represents $(100 \times t)$, m is equal to $(100 \times c)$, and p is $(10 \times l_c)$. The shapes are constructed using two polynomials, one for the thickness distribution and the other for the mean camber line. The full details of the NACA four-digit parameterization are given in Abbott and von Doenhoff [61]. A typical NACA four-digit airfoil section is shown in Fig. 10.

4.1.4 Grid Generation

The solution domain boundaries are placed at 25 chord lengths in front of the airfoil, 50 chord lengths behind it, and 25 chord lengths above and below it. The computational meshes are of structured curvilinear body-fitted C-topology with elements clustering around the airfoil and growing in size with distance from the airfoil surface. The non-dimensional normal distance (y^+) from the wall to the first grid point is roughly one. The free-stream Mach number, angle of attack, static pressure, and the turbulent viscosity ratio are prescribed at the far-field boundary. An example of a computational grid is shown in Fig. 11. The computer code ICEM CFD [62] is used for the mesh generation.

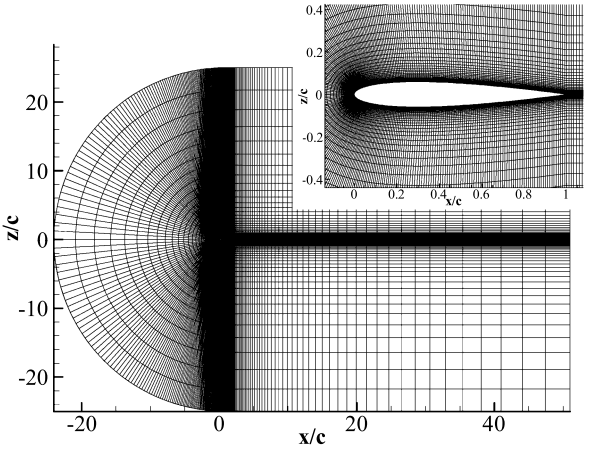

Fig. 11 An example computational grid for the NACA 0012 airfoil

4.2 Robust Airfoil Optimization Formulation

Here, the details are given for the robust aerodynamic optimization with stochastic expansions for two cases: (1) optimization under pure aleatory uncertainty and (2) optimization under mixed (aleatory and epistemic) uncertainty.

4.2.1 Optimization Under Pure Aleatory Uncertainty

The robust airfoil optimization under pure aleatory uncertainty is formulated as

$$\begin{aligned} \min \quad & \mu_{C_d} + \sigma_{C_d} \\ \text{subject to} \quad & \mu_{C_L} \geq C_L^* \\ & 0.0 \leq c \leq 0.05 \\ & 0.3 \leq l_c \leq 0.7 \\ & 0.08 \leq t \leq 0.14, \end{aligned} \tag{26}$$

where $C_d = C_d(\mathbf{X}_d, \mathbf{P}_a)$ is the profile drag coefficient, which is a function of the deterministic design variable vector $\mathbf{X}_d$ and aleatory input uncertainty vector $\mathbf{P}_a$. Similarly, the lift coefficient is $C_L = C_L(\mathbf{X}_d, \mathbf{P}_a)$. In our current optimization study, we use the deterministic design variable vector $\mathbf{X}_d = \{c, l_c, t\}$ to control our airfoil shape. Note that this vector can contain the control points as the design variables when the airfoil shape is parameterized with different spline fitting techniques. The free-stream Mach number (M_∞) is treated as aleatory (inherent) input uncertainty (i.e., $\mathbf{P}_a = \{M_\infty\}$) and represented as a uniform random variable with bounds ($0.7 \leq M_\infty \leq 0.8$). As can be seen from the Mach number range, we focus on the

transonic flow regime, where the drag coefficient is very sensitive to the changes in the Mach number due to the lambda shock originating on the top surface of the airfoil. This minimization is subject to satisfying a desired profile lift coefficient (C_L^*) value or higher by the mean value of the lift coefficient adjusted by changing the angle of attack for a given design variable and uncertain variable vector value. The optimization also includes geometric constraints for the profile shape, which bound the thickness, maximum camber, and the maximum camber location (note that l_c is taken as zero when $c = 0.0$). The drag coefficient and other aerodynamics characteristics of the airfoil for a given design variable vector and aleatory uncertain variable value are obtained from the CFD simulations that solve steady, two-dimensional, Reynolds-averaged Navier–Stokes equations with Spalart–Allmaras turbulence model.

4.2.2 Optimization Under Mixed Uncertainty

The robust airfoil optimization under mixed (aleatory and epistemic) uncertainties is formulated as

$$\begin{aligned} \min \quad & w_1 \overline{\mu}_{C_d} + w_2 \overline{\sigma}_{C_d} + w_3 \delta\sigma_{C_d} \\ \text{subject to} \quad & \mu_{C_L}^{\min} \geq C_L^* \\ & 0.0 \leq c \leq 0.05 \\ & 0.3 \leq l_c \leq 0.7 \\ & 0.08 \leq t \leq 0.14, \end{aligned} \tag{27}$$

where the profile drag coefficient $C_d(\mathbf{X}_d, \mathbf{P}_a, \mathbf{P}_e)$ is now a function of the deterministic design variable vector $\mathbf{X}_d$, aleatory input uncertainty vector $\mathbf{P}_a$, and the epistemic input uncertainty vector $\mathbf{P}_e$. Similarly, the lift coefficient, $C_L(\mathbf{X}_d, \mathbf{P}_a, \mathbf{P}_e)$, is now a function of the same variables. In the multi-objective function w_1, w_2, w_3 are the weights whose sum is equal to 1.0. In this study, we have used equal weights; however, one can choose different weights depending on the emphasis on each term.

In this optimization problem, we again consider airfoil shape parameters as our deterministic design variable vector ($\mathbf{X}_d = \{c, l_c, t\}$ and the free-stream Mach number as the aleatory (inherent) input uncertainty ($\mathbf{P}_a = \{M_\infty\}$) with bounds ($0.7 \leq M_\infty \leq 0.8$). The kinematic eddy viscosity (ν_t) obtained from the Spalart–Allmaras turbulence model used in RANS simulations is modeled as an epistemic (model-form) input uncertainty (i.e., $\mathbf{P}_e = \{\nu_t\}$) through the introduction of a factor k as shown below:

$$\nu_t = k\nu_{t_{\text{SA}}}, \tag{28}$$

where $\nu_{t_{\text{SA}}}$ is the turbulent viscosity originally obtained with the Spalart–Allmaras model. The range of this factor k is chosen between 0.5 and 2.0 to mimic the model-form uncertainty due to the use of different turbulence models in RANS calculations. Figure 12 shows the pressure distributions of a NACA 2412 airfoil at

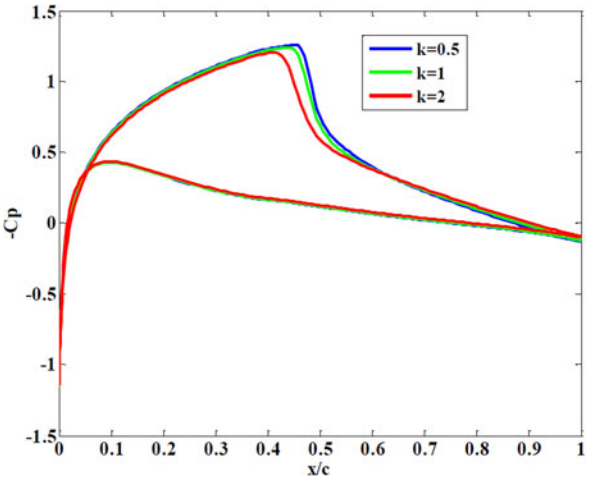

Fig. 12 The pressure distributions of NACA 2412 at $M_\infty = 0.75$, $\alpha_A = 1^\circ$

$M_\infty = 0.75$, $\alpha_A = 1^\circ$ with different k values. From this figure, it can be seen that the k factor and thus the turbulence model have a considerable effect on the pressure distribution, especially on the shock location.

This optimization is again subject to satisfying a desired profile lift coefficient (C_L^*) value or higher by the minimum of the mean value of the lift coefficient adjusted by changing the angle of attack for a given design variable and uncertain variable vector value. The optimization also includes geometric constraints for the profile shape, which bound the thickness, maximum camber, and the maximum camber location.

4.3 Utilization of Stochastic Response for Robust Optimization

Here, a stochastic response surface obtained with the point-collocation NIPC method is used for the propagation of aleatory and epistemic uncertainties due to its computational efficiency and accuracy as shown in the previous studies [43, 50]. When constructing the stochastic expansions, a combined expansion approach will be utilized, which will expand the polynomials as a function of both uncertain variables (aleatory and epistemic) and deterministic design variables.

Since the angle of attack has to be adjusted to satisfy the lift coefficient constraint in both optimization problems, we create three separate stochastic response surfaces with the point-collocation NIPC at three angles of attack ($\alpha_{A0} = 0.0^\circ$, $\alpha_{A1} = 1.0^\circ$, and $\alpha_{A2} = 2.0^\circ$). Then we apply Lagrange interpolation to create a composite response surface using these three response surfaces, which is continuous and quadratic in α_A between $\alpha_A = 0.0^\circ$ and $\alpha_A = 2.0^\circ$ for all design variables, aleatory uncertain variables (i.e., M_∞), and the epistemic uncertain variables (i.e., k). This composite response surface $\hat{R}$ (i.e., C_d or C_L), which is now a function of

α_A, $P_a(\boldsymbol{\xi}_{pa})$, $P_e(\boldsymbol{\xi}_{se})$, and $X_d(\boldsymbol{\xi}_d)$, can be written as

$$\hat{R}\big(\alpha_A, P_a(\boldsymbol{\xi}_{pa}), P_e(\boldsymbol{\xi}_{pe}), X_d(\boldsymbol{\xi}_d)\big) \cong \sum_{k=0}^{n_{\alpha_A}} R\big(P_a(\boldsymbol{\xi}_{pa}), P_e(\boldsymbol{\xi}_{pe}), X_d(\boldsymbol{\xi}_d)\big)_{\alpha_{Ak}} L_{n_{\alpha_A},k}(\alpha_A). \tag{29}$$

Based on this equation, we can slightly modify Eqs. (22) and (23) to calculate the mean and variance from $\hat{R}$:

$$\mu_{\hat{R}} = \mu_{\hat{R}}(\alpha_A, \boldsymbol{\xi}_{pe}, \boldsymbol{\xi}_d) = \sum_{k=0}^{n_{\alpha_A}} \sum_{j=0}^{P} \alpha_j(\alpha_{Ak}) L_{n_{\alpha_A},k}(\alpha_A) \big\langle \Psi_j(\boldsymbol{\xi}_{pa}, \boldsymbol{\xi}_{pe}, \boldsymbol{\xi}_d) \big\rangle_{\boldsymbol{\xi}_{pa}}, \tag{30}$$

$$\sigma^2_{\hat{R}} = \big\langle (\hat{R} - \hat{\mu_R})^2 \big\rangle_{\boldsymbol{\xi}_{pa}} = \left\{ \sum_{k=0}^{n_{\alpha_A}} \sum_{l=0}^{n_{\alpha_A}} \sum_{i=0}^{P} \sum_{j=0}^{P} L_{n_{\alpha_A},k}(\alpha_A) L_{n_{\alpha,l}}(\alpha_A) \alpha_i(\alpha_{Ak}) \alpha_j(\alpha_{Al}) \langle \Psi_i \Psi_j \rangle_{\boldsymbol{\xi}_{pa}} \right\} - \mu^2_{\hat{R}}, \tag{31}$$

where α_A is the angle of attack, $n_{\alpha_A} = 2$ is the degree of interpolation in α_A, and $L_{n_{\alpha,k}}$ is the Lagrange polynomial at α_{Ak} given by

$$L_{n_{\alpha_A},k}(\alpha_A) = \prod_{i=0, i\neq k}^{n_{\alpha_A}} \left(\frac{\alpha_A - \alpha_{Ai}}{\alpha_{Ak} - \alpha_{Ai}} \right). \tag{32}$$

Note that the introduction of α_A to the problem with the above approach indicates that it is considered as a deterministic design variable within $\hat{R}$. An alternative approach to involve α_A in the response surface would be to include it among the other deterministic design variables during the original construction.

The above formulations show that the mean and the standard deviation of response variables at a design point and angle of attack are characterized by two bounds due to epistemic uncertainties with specified interval bounds $[\mathbf{P}_e^L, \mathbf{P}_e^U]$. In other words, the mean and standard deviation of response R (i.e., C_d or C_L) at a design point and angle of attack will also be bounded by its maximum and minimum values. Once we create the composite stochastic response surface (Eq. (29)), we can use Eqs. (30) and (31) to calculate the mean and the standard deviation and use any standard optimization technique to determine $\mu_{c_d}^{\max}$, $\mu_{c_d}^{\min}$, $\sigma_{c_d}^{\max}$, and $\sigma_{c_d}^{\min}$ at a given design point and angle of attack.

With the combined expansion approach, it will be straightforward to calculate the total number of CFD simulations (N_{CFD}) required to create the composite response surface $\hat{R}$ that will be used in the entire optimization process:

$$N_{\text{CFD}} = OSR \times N_t \times (n_{\alpha_A} + 1), \tag{33}$$

where N_t is calculated from Eq. (11), and n_{α_A} is the degree of interpolation in α_A used in the creation of the composite response surface. It is important to note that N_{CFD} will be the computational cost of the described optimization approach, since once the response surface is created, the numerical evaluations at each optimization step will be computationally cheap due to the polynomial nature of the stochastic surrogate. Note that for a stochastic optimization problem with only a few design variables (i.e., $N_d \leq 3$), the combined expansion approach described above will be computationally very efficient, since a single response surface (a surrogate) is created which is a function of the design, aleatory, and epistemic uncertain variables. The optimization can be performed using this single response surface. On the other hand, in optimization problems with a large number of design variables, one can choose an alternative approach which is based on the expansion of the polynomial chaos surface only on the uncertain (aleatory and epistemic) variables. With this approach a separate stochastic response surface should be created at each design point, which will increase the computational cost; however, the accuracy of the response surface approximation will increase due to the reduction in the number of expansion variables.

4.4 Results and Discussion

The robust airfoil optimization approach with NIPC stochastic response surface is demonstrated here for two cases: (1) optimization under pure aleatory input uncertainty and (2) optimization under mixed (aleatory and epistemic) uncertainty.

4.4.1 Optimization Results for the Pure Aleatory Uncertainty Case

The free-stream Mach number is the only uncertain variable for this case and modeled with a uniform probability distribution between $M_\infty = 0.7$ and $M_\infty = 0.8$. The objective (Eq. (26)) is to reduce the mean and the standard deviation of the drag coefficient simultaneously to obtain an airfoil shape with minimum drag that is least sensitive to the change in Mach number in the specified range. Besides the side (geometric) constraints on the design variables, the minimization is performed such that the mean lift coefficient obtained with the optimum design is greater than or equal to 0.5. The stochastic response surfaces for the drag and the lift coefficients were created with the point-collocation NIPC method using a quadratic polynomial expansion with an OSR of 2 for four variables (three deterministic design variables and one uncertain variable). The total number of CFD evaluations required for this case was $N_{\text{CFD}} = 90$, as can be calculated using Eq. (33) along with Eq. (11). Note that this number is considerably low compared to the cost of alternative robust optimization formulations, which utilize Monte Carlo simulations for the calculation of the statistics. After the stochastic response surfaces for the drag and lift coefficients

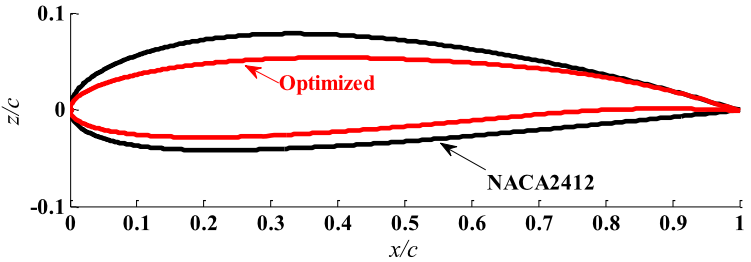

Fig. 13 NACA 2412 and the optimized airfoil shapes for the pure aleatory uncertainty case

Table 5 Optimization results for the pure aleatory uncertainty case

	Initial airfoil			Optimized airfoil		
	c	l_c	t	c	l_c	t
NACA 2412	0.020	0.40	0.120	0.0195	0.70	0.080
NACA 0012	0.0	0.0	0.120	0.0195	0.70	0.080

are created, the robust optimization is performed using the approach described in the previous section.

The robust optimization was performed starting from two different initial airfoil geometries (NACA 2412 and NACA 0012). As can be seen from Table 5, both optimization runs converged to the same optimum airfoil shape with $t = 0.08$, $c = 0.0195$, and $l_c = 0.7$ (Fig. 13). The optimum airfoil has the minimum thickness allowable and the camber is located as aft as possible toreduce the drag while satisfying the required C_L, which are typical characteristics of airfoils designed to operate at transonic speeds (e.g., supercritical airfoils). The camber value is the optimum to produce the required lift at an optimum angle of attack.

The pressure distributions of the NACA 2412 and optimum airfoils at $M_\infty = 0.75$ are shown in Fig. 14. From this figure we can see that, at $M_\infty = 0.75$, the NACA 2412 airfoil has a shock wave on the top surface, whereas no shock wave exists on the optimized airfoil, due to the increase in minimum suction pressure (i.e., the decrease of the maximum value of $-C_p$) and the reduction in the maximum velocity value on the top surface, giving a more flat pressure distribution. The aft camber compensates the lift that is lost in the suction region by loading the airfoil in the aft region.

The optimization history of the mean and the standard deviation of the drag coefficient is given in Fig. 15, which shows that both quantities are minimized simultaneously regardless of the initial airfoil chosen, which confirms the robust optimization approach used. This result is further verified by Fig. 16, which gives drag versus Mach number over the uncertain Mach number range for the NACA 2412 and optimized airfoil at a lift coefficient value of 0.5. As can be seen from this plot, the drag rise of NACA 2412 is significant, whereas the optimum airfoil maintains a low drag coefficient value over the uncertain Mach number range with no significant variation. The drag coefficient and L/D values for both airfoils are reported in Ta-

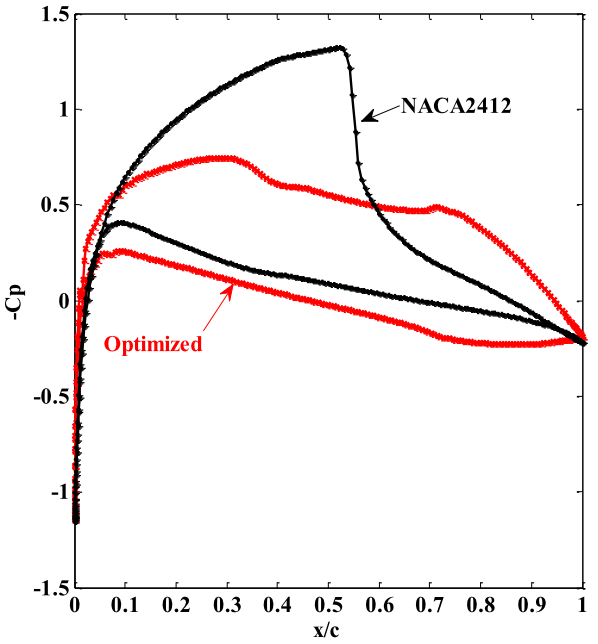

Fig. 14 The pressure distributions of NACA 2412 and optimum airfoil at $M_\infty = 0.75$ for the pure aleatory uncertainty case

ble 6, which quantifies the better aerodynamic performance of the optimum airfoil compared to NACA 2412.

The drag characteristics of both airfoils can also be explained by examining the Mach number contours given in Fig. 17. As the Mach number increases, the shock wave on the top surface of the NACA 2412 airfoil gets stronger and eventually induces the boundary layer separation at a free-stream Mach number of 0.8, increasing the drag significantly. On the other hand, the delayed shock formation on the top surface of the optimum airfoil shape prevents a significant drag rise over the uncertain Mach number range considered. The pressure distributions of the NACA 2412 and optimum airfoils at $M_\infty = 0.7$, 0.75, and 0.8 are shown in Fig. 18. It can be seen that at $M_\infty = 0.7$, 0.75, the NACA 2412 airfoil has a shock wave on the top surface, whereas no shock wave exists on the optimized airfoil. At $M_\infty = 0.8$, the shock wave on the optimized airfoil is much weaker compared to the shock on the NACA 2412 airfoil.

4.4.2 Optimization Results for the Mixed Uncertainty Case

As described with the optimization formulation in Sect. 4.2.2, the free-stream Mach number is taken as the aleatory uncertain variable for this case and modeled with a uniform probability distribution between $M_\infty = 0.7$ and $M_\infty = 0.8$, the same

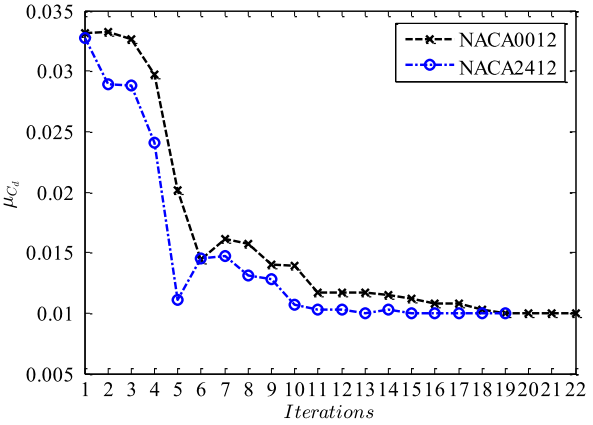

(a) Mean drag coefficient, μ_{C_d}

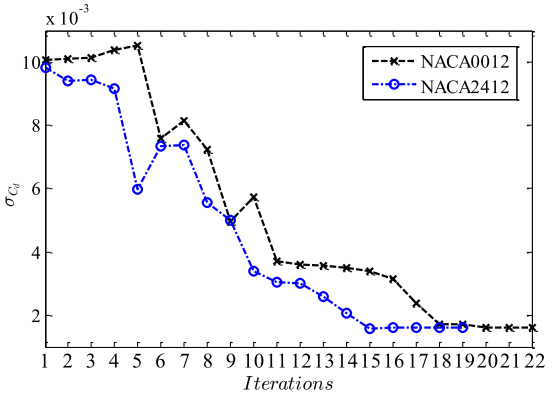

(b) Standard deviation, σ_{C_d}

Fig. 15 The optimization history of the mean and the standard deviation of the drag coefficient for the pure aleatory uncertainty case starting from two initial airfoil shapes (NACA 2412 and NACA 0012)

as in the pure aleatory case. The k factor, which is multiplied by the turbulent eddy-viscosity coefficient of the Spalart–Allmaras turbulence model, is the epistemic uncertain variable defined with the interval $[0.5, 2.0]$. The objective of the robust optimization under mixed uncertainties (Eq. (27)) is to reduce the average of the mean ($\bar{\mu}_{C_d}$), the average of the standard deviation ($\bar{\sigma}_{C_d}$), and the difference in the standard deviation of the drag coefficient ($\delta\sigma_{C_d}$) simultaneously to obtain an airfoil shape with minimum drag that is least sensitive to the change in Mach number and the k factor (i.e., the turbulence model) in the range specified for each variable. Besides the side (geometric) constraints on the design variables, the minimization is performed such that the minimum of the mean lift coefficient obtained with the optimum design is greater than or equal to 0.5. The stochastic response surfaces for the drag and the lift coefficients were again created with point-collocation

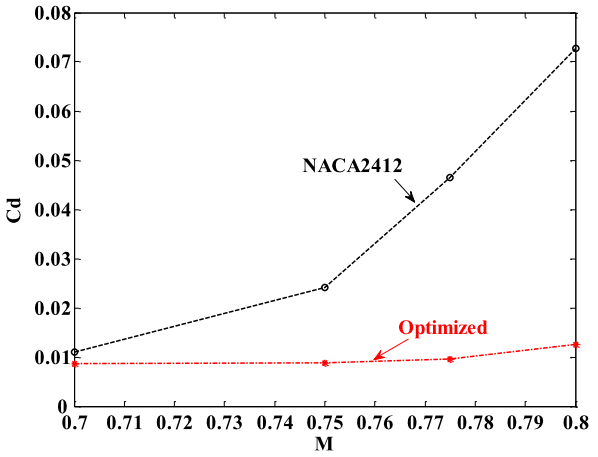

Fig. 16 The drag coefficients of the NACA 2412 and optimized airfoils at $C_L^* = 0.5$

Table 6 Drag coefficient and L/D values for NACA 2412 and optimum airfoils at various Mach numbers for pure aleatory uncertainty case

M	C_d		L/D	
	NACA 2412	Optimized	NACA 2412	Optimized
0.7	0.0110	0.0086	45.45	58.14
0.75	0.0242	0.0088	20.66	56.82
0.8	0.0727	0.0126	6.88	39.68

NIPC using a quadratic polynomial expansion with an OSR of 2 for five variables (three deterministic design variables, one aleatory uncertain variable, and one epistemic uncertain variable). The total number of CFD evaluations required for this case was $N_{\text{CFD}} = 126$, as can be calculated using Eq. (33) along with Eq. (11). Because we consider the propagation of an aleatory and epistemic uncertain variable simultaneously, this number signifies the computational efficiency of the proposed optimization approach. After the stochastic response surfaces for the drag and lift coefficients are created, the robust optimization is performed using the approach described in the previous section. As a result of the optimization under mixed uncertainties, the same optimum airfoil shape as in the pure aleatory uncertainty case is obtained (Table 7). This optimum has been verified by starting the optimization from two different initial profile shapes (NACA 2412 and NACA 0012). This result is somehow expected, since the flow field around the optimum airfoil shape does not include complex flow features such as strong shocks and shock-induced separation over the range of Mach numbers considered to make the effect of the turbulence model (i.e., the k factor) significant on different aerodynamic quantities including the drag coefficient.

Figure 19 gives the convergence history of the average mean, average standard deviation, and the difference of the drag coefficient for the mixed uncertainty case starting from two initial airfoil shapes (NACA 2412 and NACA 0012). Regardless

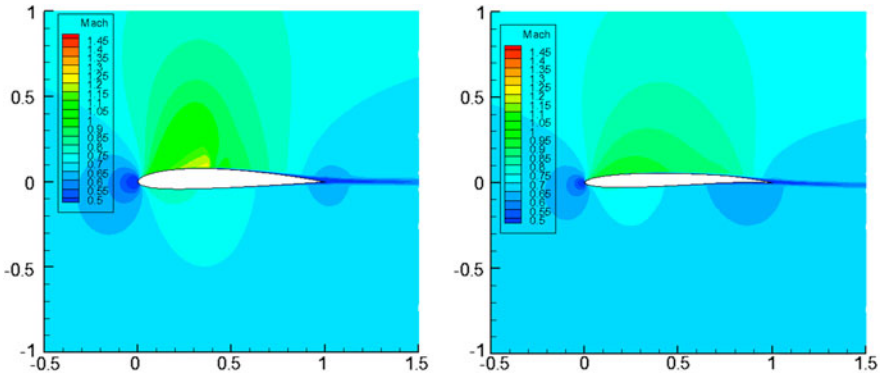

(a) $M_\infty = 0.7$, NACA 2412 (b) $M_\infty = 0.7$, Optimum airfoil

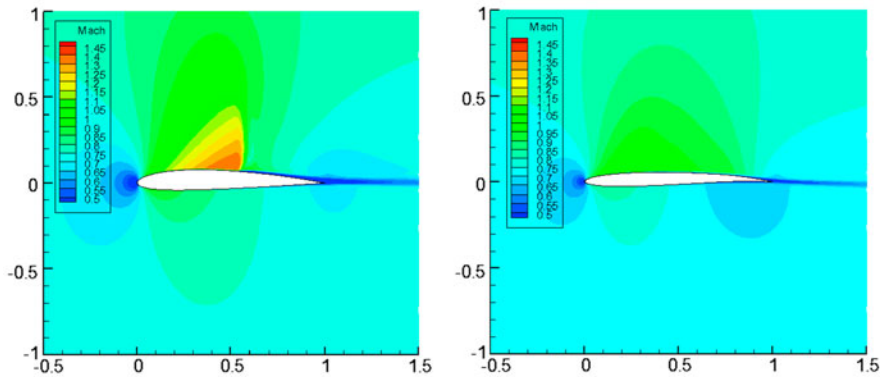

(c) $M_\infty = 0.75$, NACA 2412 (d) $M_\infty = 0.75$, Optimum airfoil

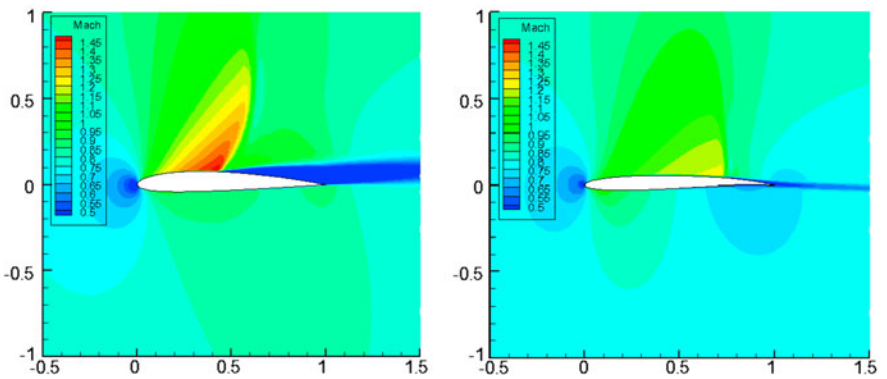

(e) $M_\infty = 0.8$, NACA 2412 (f) $M_\infty = 0.8$, Optimum airfoil

Fig. 17 Mach number contours for the NACA 2412 and optimum airfoil shapes for the pure aleatory uncertainty case

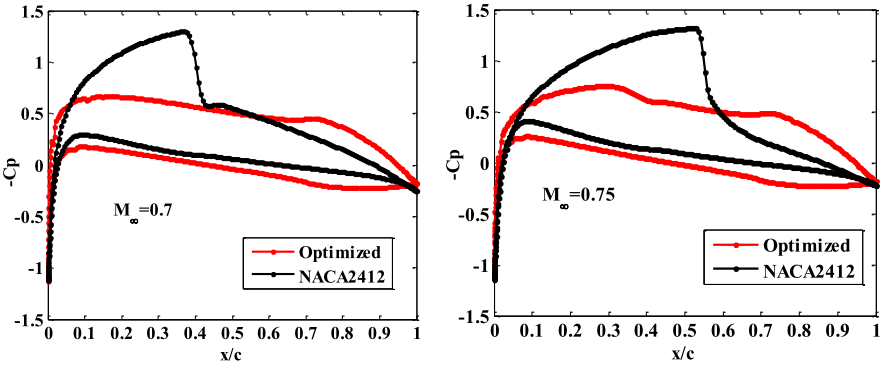

(a) $M_\infty = 0.7$ (b) $M_\infty = 0.75$

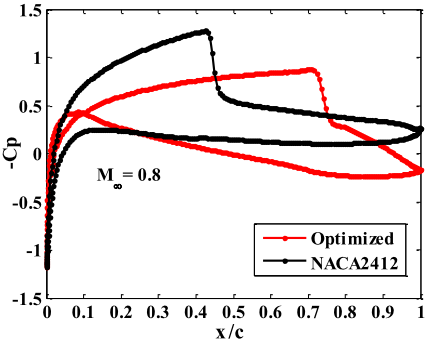

(c) $M_\infty = 0.8$

Fig. 18 The pressure distributions of the NACA 2412 and optimum airfoils at $M_\infty = 0.7$, 0.75, 0.8 for the pure aleatory uncertainty case

Table 7 Optimization results for the mixed uncertainty case

	Initial airfoil			Optimized airfoil		
	c	l_c	t	c	l_c	t
NACA 2412	0.020	0.400	0.120	0.019	0.700	0.080
NACA 0012	0	0	0.120	0.019	0.700	0.080

of the initial airfoil geometry used, all three quantities are reduced compared to their starting values and converge to the same final values. On the other hand, the reduction in the average mean and the average standard deviation of the drag coefficient is larger compared to the reduction in the difference of the standard deviation, which already has a small value for the initial airfoil shapes considered. This observation may imply that, for this optimization problem, the contribution of the epistemic uncertainty (i.e., k factor) is not as much as the contribution of the aleatory uncertainty (Mach number) to the total uncertainty in the drag coefficient. Since the optimiza-

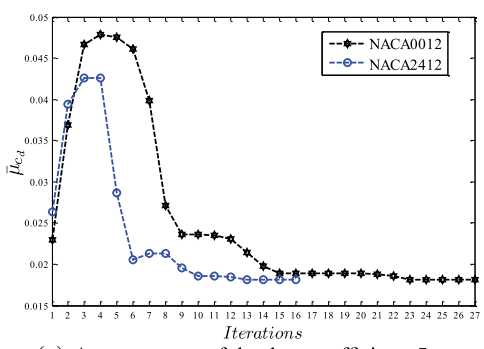

(a) Average mean of the drag coefficient, $\bar{\mu}_{C_d}$

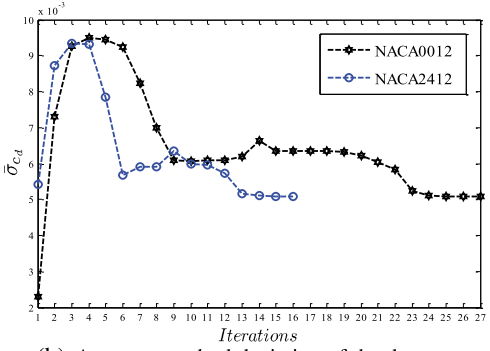

(b) Average standard deviation of the drag coefficient, $\bar{\sigma}_{C_d}$

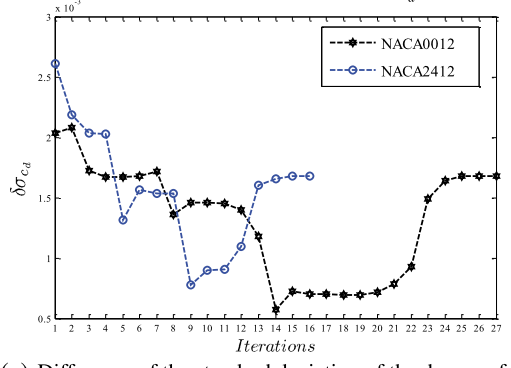

(c) Difference of the standard deviation of the drag coefficient, $\delta\sigma_{C_d}$

Fig. 19 The optimization history of average mean, average standard deviation, and the difference of the drag coefficient for the mixed uncertainty case starting from two initial airfoil shapes (NACA 2412 and NACA 0012)

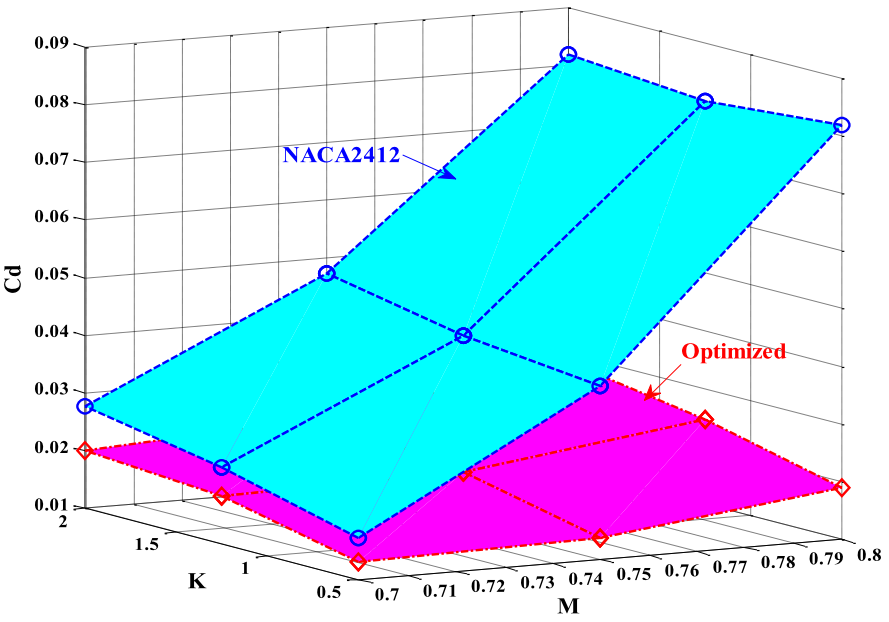

Fig. 20 Drag coefficient values of the optimized airfoil and NACA 2412 for $M_\infty = [0.7, 0.75, 0.8]$ and $k = [0.5, 1.25, 2.0]$ at $C_L^* = 0.5$

tion is performed at a relatively low lift coefficient value ($C_L^* = 0.5$), one may also expect to see more contribution from the epistemic uncertainty at higher lift coefficients. Figure 20, which shows a carpet plot of the drag coefficient over the range of M_∞ and the k factor considered, also verifies that the aerodynamic characteristics of the optimum airfoil are better compared to the characteristics of NACA 2412 (one of the airfoils used to initiate the optimization) in the case of mixed uncertainties, and no significant drag rise (i.e., variation) is observed with the optimum geometry. This plot also shows that the uncertainty in the Mach number is the main contributor to the overall uncertainty and variation in the drag coefficient, which can be quantified by the results tabulated in Table 8.

5 Conclusions

This chapter described the utilization of a computationally efficient uncertainty quantification (UQ) approach and NIPC-based stochastic expansions in robust design under mixed (aleatory and epistemic) uncertainties and demonstrated this technique on a model problem and robust aerodynamic optimization.

The optimization approach utilized stochastic response surfaces obtained with NIPC methods to approximate the objective function and the constraints in the optimization formulation. The objective function includes stochastic measures, which

Table 8 Drag coefficient and L/D values for NACA 2412 and optimum airfoils at various Mach numbers and k values for the mixed uncertainty case

K	M_∞	C_d		L/D	
		NACA 2412	Optimized	NACA 2412	Optimized
$K = 0.5$	0.7	0.0171	0.0131	29.22	38.17
	0.75	0.0401	0.0136	12.48	36.76
	0.8	0.0819	0.0189	6.11	26.48
$K = 1.25$	0.7	0.0233	0.0184	21.46	27.21
	0.75	0.0427	0.0190	11.71	26.37
	0.8	0.0798	0.0248	6.26	20.16
$K = 2.0$	0.7	0.0277	0.0201	18.07	24.88
	0.75	0.0474	0.0224	10.55	22.32
	0.8	0.0817	0.0286	6.12	17.51

are minimized simultaneously to ensure the robustness of the final design to both aleatory and epistemic uncertainties. The optimization approach was first demonstrated on the robust design of a beam under mixed uncertainties. The stochastic expansions are created with two different NIPC methods, quadrature-based and point-collocation NIPC. The optimization results were compared to the results of another robust optimization technique that utilized double-loop Monte Carlo sampling for the propagation mixed uncertainties. The results obtained with the two different optimization approaches agreed well; however, the number of function evaluations was much less than the number required by the Monte Carlo-based approach, indicating the computational efficiency of the described optimization technique.

For robust aerodynamic optimization under aleatory (Mach number) and epistemic (turbulence model) uncertainties, the NIPC response surface was also used as the basis for surrogates in the optimization process. To create the surrogates, a combined point-collocation NIPC approach was utilized, which was a function of both the design and uncertain variables. Two stochastic optimization formulations were studied: (1) optimization under pure aleatory uncertainty and (2) optimization under mixed (aleatory and epistemic) uncertainty. The formulations were demonstrated for the drag minimization of NACA four-digit airfoils described with three geometric design variables over the range of uncertainties under transonic flow conditions. Deterministic CFD simulations were performed to solve steady, two-dimensional, compressible, turbulent RANS equations. The pure aleatory uncertainty case included the Mach number as the uncertain variable. For the mixed uncertainty case, a k factor, which is multiplied by the turbulent eddy-viscosity coefficient, is introduced to the problem as the epistemic uncertain variable. The results of both optimization cases confirmed the effectiveness of the robust optimization approach with stochastic expansions by giving an optimum airfoil shape that has the minimum drag over the range of aleatory and epistemic uncertainties. The optimization under pure aleatory uncertainty case required 90 deterministic CFD evaluations,

whereas the optimization under mixed uncertainty case required 126 CFD evaluations to create the stochastic response surfaces, which show the computational efficiency of the stochastic optimization with stochastic expansions. Note also that the stochastic optimization methodology described in this chapter is general in the sense that it can be applied to any robust design problem in science and engineering.

References

1. Taguchi, G., Chowdhury, S., Taguchi, S.: Robust Engineering. McGraw-Hill, New York (2000)
2. Taguchi, G.: Taguchi on Robust Technology Development: Bringing Quality Engineering Upstream. ASME Press, New York (1993)
3. Papadimitriou, D.I., Giannakoglou, K.C.: Third-order sensitivity analysis for robust aerodynamic design using continuous adjoint. Int. J. Numer. Methods Fluids (2012)
4. Wiebenga, J.H., Van Den Boogaard, A.H., Klaseboer, G.: Sequential robust optimization of a V-bending process using numerical simulations. Struct. Multidiscip. Optim. **46**(1), 137–153 (2012)
5. Du, X., Chen, W.: Efficient uncertainty analysis methods for multidisciplinary robust design. AIAA J. **40**(3), 545–552 (2002)
6. Karpel, M., Moulin, B., Idan, M.: Robust aeroservoelastic design with structural variations and modeling uncertainties. J. Aircr. **40**(5), 946–954 (2003)
7. Ramakrishnan, B., Rao, S.S.: A general loss function based optimization procedure for robust design. Eng. Optim. **25**(4), 255–276 (1996)
8. Patel, J., Kumar, A., Allen, J.K., Ruderman, A., Choi, S.K.: Variable sensitivity-based deterministic robust design for nonlinear system. J. Mech. Des. **132**, 0645021 (2010)
9. Choi, H., McDowell, D.L., Allen, J.K., Rosen, D., Mistree, F.: An inductive design exploration method for robust multiscale materials design. J. Mech. Des. **130**(3) (2008)
10. Ruderman, A., Choi, S.-K., Patel, J., Kumar, A., Allen, J.K.: Simulation-based robust design of multiscale products. J. Mech. Des. **132**(10) (2010)
11. Ray, T., Saha, A.: Practical robust design optimization using evolutionary algorithms. J. Mech. Des. **133** (2011)
12. Li, H.X., Lu, X.: Perturbation theory based robust design under model uncertainty. J. Mech. Des. **131**, 1110061 (2009)
13. Beyer, H.-G., Sendhoff, B.: Robust optimization−a comprehensive survey. Comput. Methods Appl. Mech. Eng. **196**(33–34), 3190–3218 (2007)
14. Fishman, G.S.: Monte Carlo: Concepts, Algorithms, and Applications. Springer, New York (1995). ISBN 0-387-94527-X
15. Kroese, D.P., Taimre, T., Botev, Z.I.: Handbook of Monte Carlo Methods, p. 772. Wiley, New York (2011). ISBN 0-470-17793-4
16. Siebert, B.R.L., Cox, M.G.: The use of a Monte Carlo method for evaluating uncertainty and expanded uncertainty. Metrologia **43**(4), S178–S188 (2006)
17. Zhao, L.Y., Zhang, X.Q.: Uncertainty quantification of a flapping airfoil with a stochastic velocity deviation based on a surrogate model. Adv. Mater. Res. **201–203**, 1209–1212 (2011)
18. Zhao, L., Zhang, X.: Uncertainty quantification of a flapping airfoil with stochastic velocity deviations using the response surface method. Open Mech. Eng. J. **5**(1), 152–159 (2011)
19. Du, X.: Unified uncertainty analysis by the first order reliability method. J. Mech. Des. **130**(9), 0914011 (2008)
20. Sujecki, S.: Extended Taylor series and interpolation of physically meaningful functions. Opt. Quantum Electron., 1–14 (2012)

21. Chen, Z.-J., Xiao, H.: The Taylor series multipole boundary element method (TSM-BEM) and its applications in rolling engineering. Chongqing Daxue Xuebao **35**(5), 57–63 (2012)
22. Shu, C., Peng, Y., Zhou, C.F., Chew, Y.T.: Application of Taylor series expansion and least-squares-based lattice Boltzmann method to simulate turbulent flows. J. Turbul. **7**, 1–12 (2006)
23. Rahman, S., Rao, B.N.: A perturbation method for stochastic meshless analysis in elastostatics. Int. J. Numer. Methods Eng. **50**, 1961–1991 (2001)
24. Waiboer, R.R., Aarts, R.G.K.M., Jonker, J.B.: Application of a perturbation method for realistic dynamic simulation of industrial robots. Multibody Syst. Dyn. **13**(3), 323–338 (2005)
25. Khattri, S.K.: Series expansion of functions with He's homotopy perturbation method. Int. J. Math. Educ. Sci. Technol. **43**(5), 677–684 (2012)
26. Lee, S.H., Chen, W.: A comparative study of uncertainty propagation methods for black-box-type problems. Struct. Multidiscip. Optim. **37**(3), 239–253 (2009)
27. Eldred, M.S., Webster, C.G., Constantine, P.G.: Evaluation of non-intrusive approaches for Wiener-Askey generalized polynomial chaos. In: 10th AIAA Non-deterministic Approaches Forum, Schaumburg, IL (2008). AIAA-paper 2008-1892
28. Eldred, M.S., Burkardt, J.: Comparison of non-intrusive polynomial chaos and stochastic collocation methods for uncertainty quantification. In: 47th AIAA Aerospace Sciences Meeting, Orlando, FL, January (2009). AIAA 2009-0976
29. Veneziano, D., Agarwal, A., Karaca, E.: Decision making with epistemic uncertainty under safety constraints: an application to seismic design. Probab. Eng. Mech. **24**(3), 426–437 (2009)
30. Huang, H.-Z., Zhang, X.: Design optimization with discrete and continuous variables of aleatory and epistemic uncertainties. J. Mech. Des. **131**(3), 0310061 (2009)
31. Dolšek, M.: Simplified method for seismic risk assessment of buildings with consideration of aleatory and epistemic uncertainty. Struct. Infrastruct. Eng. **8**(10), 939–953 (2012)
32. Swiler, L.P., Paez, T., Mayes, R.: Epistemic uncertainty quantification tutorial. In: SAND 2008-6578C, Paper 294 in the Proceedings of the IMAC XXVII Conference and Exposition on Structural Dynamics, Society for Structural Mechanics, Orlando, FL, Feb. (2009)
33. Swiler, L., Paez, T., Mayes, R., Eldred, M.: Epistemic uncertainty in the calculation of margins. In: 50th AIAA/ASME/ASCE/AHS/ASC Structures, Structural Dynamics, and Materials Conference, Palm Springs, CA, May (2009). AIAA 2009-2249
34. Du, X.: Reliability-based design optimization with dependent interval variables. Int. J. Numer. Methods Eng. **91**(2), 218–228 (2012)
35. Ju, Y.P., Zhang, C.H.: Multi-point robust design optimization of wind turbine airfoil under geometric uncertainty. Proc. Inst. Mech. Eng. A, J. Power Energy **226**(2), 245–261 (2012)
36. Haro Sandoval, E., Anstett-Collin, F., Basset, M.: Sensitivity study of dynamic systems using polynomial chaos. Reliab. Eng. Syst. Saf. **104**, 15–26 (2012)
37. Didier, J., Faverjon, B., Sinou, J.-J.: Analysing the dynamic response of a rotor system under uncertain parameters by polynomial chaos expansion. J. Vib. Control **18**(5), 712–732 (2012)
38. Cheng, H., Sandu, A.: Efficient uncertainty quantification with the polynomial chaos method for stiff systems. Math. Comput. Simul. **79**(11), 3278–3295 (2009)
39. Hosder, S., Walters, R.W., Balch, M.: Efficient sampling for non-intrusive polynomial chaos applications with multiple input uncertain variables
40. Hosder, S., Walters, R.W., Perez, R.: A non-intrusive polynomial chaos method for uncertainty propagation in CFD simulations. In: 44th AIAA Aerospace Sciences Meeting and Exhibit, Reno, Nevada, January (2006). AIAA 2006-891
41. Bettis, B., Hosder, S.: Quantification of uncertainty in aerodynamic heating of a reentry vehicle due to uncertain wall and freestream conditions. In: 10th AIAA Joint Thermophysics and Heat Transfer Conference, Chicago, IL, June (2010). AIAA 2010-4642
42. Eldred, M.S., Swiler, L.P., Tang, G.: Mixed aleatory-epistemic uncertainty quantification with stochastic expansions and optimization-based interval estimation. Reliab. Eng. Syst. Saf. **96**(9), 1092–1113 (2011)
43. Hosder, S., Bettis, B.: Uncertainty and sensitivity analysis for reentry flows with inherent and model-form uncertainties. J. Spacecr. Rockets **49**(2), 193–206 (2012)

44. Eldred, M.S.: Design under uncertainty employing stochastic expansion methods. Int. J. Uncertain. Quantif. **1**(2), 119–146 (2011)
45. Dodson, M., Parks, G.T.: Robust aerodynamic design optimization using polynomial chaos. J. Aircr. **46**(2), 635–646 (2009)
46. Youn, B.D., Choi, K.K., Du, L., Gorsich, D.: Integration of possibility-based optimization and robust design for epistemic uncertainty. J. Mech. Des. **129**(8), 876–882 (2007)
47. Eldred, M.S.: Recent advances in non-intrusive polynomial chaos and stochastic collocation methods for uncertainty analysis and design (2009)
48. Du, X., Venigella, P.K., Liu, D.: Robust mechanism synthesis with random and interval variables. Mech. Mach. Theory **44**(7), 1321–1337 (2009)
49. Zhang, Y., Hosder, S., Leifsson, L., Koziel, S.: Robust airfoil optimization under inherent and model-form uncertainties using stochastic expansions. In: 50th AIAA Aerospace Sciences Meeting Including the New Horizons Forum and Aerospace Exposition, Nashville, TN, January 9–12 (2012). AIAA 2012-0056
50. Hosder, S., Walters, R.W., Balch, M.: Point-collocation nonintrusive polynomial chaos method for stochastic computational fluid dynamics. AIAA J. **48**(12), 2721–2730 (2010)
51. Wiener, N.: The homogeneous chaos. Am. J. Math. **60**(4), 897–936 (1994)
52. Xiu, D., Karniadakis, G.E.: Modeling uncertainty in flow simulations via generalized polynomial chaos. J. Comput. Phys. **187**(1), 137–167 (2003)
53. Walters, R.W., Huyse, L.: Uncertainty analysis for fluid mechanics with applications. Technical report, ICASE 2002-1, NASA/CR-2002-211449, NASA Langley Research Center, Hampton, VA (2002)
54. Najm, H.N.: Uncertainty quantification and polynomial chaos techniques in computational fluid dynamics. Annu. Rev. Fluid Mech. **41**, 35–52 (2009)
55. Hosder, S., Walters, R.W.: Non-intrusive polynomial chaos methods for uncertainty quantification in fluid dynamics. In: 48th AIAA Aerospace Sciences Meeting, Orlando, FL, January 4–7 (2010). AIAA-paper 2010-0129
56. Hosder, S., Walters, R.W., Balch, M.: Efficient sampling for non-intrusive polynomial chaos applications with multiple input uncertain variables. In: 9th AIAA Non-deterministic Approaches Conference, Honolulu, HI, April (2007). AIAA-paper 2007-1939
57. Vanderplaats, G.N.: Numerical Optimization Techniques for Engineering Design, 3rd edn. Vanderplaats Research and Development, Colorado Springs (1999)
58. Anderson, J.D.: Fundamentals of Aerodynamics, 4th edn. McGraw-Hill, New York (2010)
59. Spalart, P.R., Allmaras, S.R.: A one equation turbulence model for aerodynamic flows. In: 38th AIAA Aerospace Sciences Meeting and Exhibit, Reno, Nevada, January 6–9 (1992). AIAA-paper-92-0439
60. FLUENT, ver. 13.0. ANSYS Inc., Southpointe, 275 Technology Drive, Canonsburg, PA, 15317 (2011)
61. Abbott, I.H., Von Doenhoff, A.E.: Theory of Wing Sections. Dover Publications, Mineola (1959)
62. ICEM CFD, ver. 13.0. ANSYS Inc., Southpointe, 275 Technology Drive, Canonsburg, PA 15317 (2011)